

NIST Series Technical Note 2185

Thermal and gas mixture composition measurements preceding backdrafts in a 2/5th scale compartment

Draft Stage

Ryan Falkenstein-Smith Thomas Cleary

This publication is available free of charge from:
<https://doi.org/10.6028/NIST.XXX.XXXX>



NIST Series Technical Note 2185

Thermal and gas mixture composition measurements preceding backdrafts in a 2/5th scale compartment

Draft Stage

Ryan Falkenstein-Smith
Thomas Cleary
Fire Research Division
Engineering Laboratory

This publication is available free of charge from:
<https://doi.org/10.6028/NIST.XXX.XXXX>

September 2022



U.S. Department of Commerce
Gina M. Raimondo, Secretary

National Institute of Standards and Technology
Laurie E. Locascio, NIST Director and Under Secretary of Commerce for Standards and Technology

³² Certain commercial entities, equipment, or materials may be identified in this document in order to describe
³³ an experimental procedure or concept adequately. Such identification is not intended to imply
³⁴ recommendation or endorsement by the National Institute of Standards and Technology, nor is it intended to
³⁵ imply that the entities, materials, or equipment are necessarily the best available for the purpose.

³⁶ **NIST Technical Series Policies**
³⁷ [Copyright, Fair Use, and Licensing Statements](#)
³⁸ [NIST Technical Series Publication Identifier Syntax](#)

³⁹ **How to cite this NIST Technical Series Publication:**
⁴⁰ Ryan Falkenstein-Smith, Thomas Cleary (2022) Thermal and gas mixture composition measurements
⁴¹ preceding backdrafts in a 2/5th scale compartment. (National Institute of Standards and Technology,
⁴² Gaithersburg, MD), 2185. <https://doi.org/10.6028/NIST.XXX.XXXX>

⁴³ **NIST Author ORCID iDs**
⁴⁴ Ryan Falkenstein-Smith: 0000-0001-7039-5835
⁴⁵ Thomas Cleary: 0000-0001-8785-2035

⁴⁶ **Contact Information**
⁴⁷ ryan.falkenstein-smith@nist.gov

⁴⁸ **Abstract**

⁴⁹ This report documents real-time and time-averaged temperature, global and local equivalence ratios, and oxygen, carbon dioxide, and carbon monoxide concentration measurements made at various positions in an isolated 2/5th scale compartment, prior to a backdraft event. The compartment was subjected to methane, propane, and propylene fires of different sizes and fuel flow times. Backdrafts were observed to vary depending on the fuel source. Gas mixture composition measurements obtained prior to an anticipated backdraft were obtained through various gas analysis techniques, including an enhanced phi meter, a gas analyzer equipped with a paramagnetic and two non-dispersive infrared sensors, and a Gas Chromatograph/Mass Spectrometer System. Measurements and the influence of transient compartment conditions including opening configuration, spark igniter location, fire size, and fuel flow time are discussed in detail. The likelihood of backdraft under these compartment configurations is typically improved with a higher spark igniter location and fire size, smaller compartment opening and shorter fuel flow time.

⁶² **Key words**

⁶³ Backdraft; Gas Species Concentrations; Global Equivalence Ratio; Local Equivalence Ratio;
⁶⁴ Reduced-Scale Enclosure; Real-time Measurements; Time-averaged Measurements.

67

Table of Contents

68 1. Introduction	1
69 2. Description of Experiments	1
70 2.1. Compartment configuration	1
71 2.2. Experimental procedure	2
72 2.3. Gas composition measurements	4
73 3. Results	6
74 3.1. Temperature measurements	6
75 3.1.1. Real-Time temperature measurements	6
76 3.1.2. Time-Averaged temperature measurements	10
77 3.2. Gas mixture composition measurements	14
78 3.2.1. Real-Time gas mixture composition measurements	14
79 3.2.2. Time-Averaged gas mixture composition measurements	21
80 4. Verifying Gas Composition Measurements	29
81 5. Probabilities of Backdraft at varying experimental conditions	31
82 6. Conclusion	39
83 References	40
84 Appendix A. Uncertainty Analysis of Real-time Measurements	42
85 A.1. Temperature	42
86 A.2. Gas Species Concentration Measurements obtained via Gas Analyzer . . .	42
87 A.3. Global Equivalence Ratio	42
88 A.4. Local Equivalence Ratio	43
89 Appendix B. Uncertainty Analysis of Time-Averaged Measurements	44

90

List of Tables

91 Table 1. List of fuel flow times for each fire configuration	4
92 Table 2. List of uncertainties for gas analyzer components.	42
93 Table 3. List of uncertainties for selected phi meter components.	43

94

List of Figures

95 Fig. 1. Schematic of the 2/5 th scale compartment utilized for backdraft experiments.	3
---	---

96	Fig. 2.	Real-time temperature measurements of the 25.0 kW, 31.3 kW, and 37.5 kW methane fires within the compartment prior to backdraft	7
97	Fig. 3.	Real-time temperature measurements of the 16.7 kW, 20.9 kW, and 25.0 kW propane fires within the compartment prior to backdraft	8
99	Fig. 4.	Real-time temperature measurements of a 25.0 kW propylene fire within the compartment prior to backdraft	9
100	Fig. 5.	Time-averaged temperature measurements of the 25.0 kW, 31.3 kW, and 37.5 kW methane fires within the compartment prior to backdraft	11
102	Fig. 6.	Time-averaged temperature measurements of the 16.7 kW, 20.9 kW, and 25.0 kW propane fires within the compartment prior to backdraft	12
104	Fig. 7.	Time-averaged temperature measurements of the 25.0 kW propylene fire within the compartment prior to backdraft	13
108	Fig. 8.	Real-time gas mixture composition measurements of the 25.0 kW, 31.3 kW, and 37.5 kW methane fires within the compartment prior to backdraft	17
110	Fig. 9.	Sequences of flame propagation in the compartment previously subjected to 25.0 kW methane, propane, and propylene fires with a fuel flow time of 450 s, 300 s, 270 s, respectively.	18
113	Fig. 10.	Real-time gas mixture composition measurements of the 16.7 kW, 20.9 kW, and 25.0 kW propane fires within the compartment prior to backdraft	19
115	Fig. 11.	Real-time gas mixture composition measurements of a 25.0 kW propylene fire within the compartment prior to backdraft	20
117	Fig. 12.	Time-averaged gas mixture composition measurements of the 25.0 kW, 31.3 kW, and 37.5 kW methane fires within the compartment prior to backdraft	22
120	Fig. 13.	Time-averaged gas mixture composition measurements of the 16.7 kW, 20.9 kW, and 25.0 kW propane fires within the compartment prior to back- draft	23
123	Fig. 14.	Time-averaged gas mixture composition measurements of the 25.0 kW propylene fire within the compartment prior to backdraft	24
125	Fig. 15.	Time-averaged gas species concentration measurements obtained via GC/MSD of the 25.0 kW, 31.3 kW, and 37.5 kW methane fires within the compart- ment prior to backdraft	26
128	Fig. 16.	Time-averaged gas species concentration measurements obtained via GC/MSD of the 16.7 kW, 20.9 kW, and 25.0 kW propane fires within the compart- ment prior to backdraft	27
131	Fig. 17.	Time-averaged gas species concentration measurements obtained via GC/MSD of the 25.0 kW propylene fires within the compartment prior to backdraft	28
133	Fig. 18.	Time-averaged gas mixture composition measurements obtained via phi meter and gas analyzers compared against time-averaged measurements made via GC/MSD	30
136	Fig. 19.	Conditional density plot of a 25 kW methane fire as a function of fuel flow time at various compartment configurations	32
138	Fig. 20.	Conditional density plot of a 31.3 kW methane fire as a function of fuel flow time at various compartment configurations	33

140	Fig. 21. Conditional density plot of a 37.5 kW methane fire as a function of fuel	
141	flow time at various compartment configurations	34
142	Fig. 22. Conditional density plot of a 16.7 kW propane fire as a function of fuel	
143	flow time at various compartment configurations	35
144	Fig. 23. Conditional density plot of a 20.9 kW propane fire as a function of fuel	
145	flow time at various compartment configurations	36
146	Fig. 24. Conditional density plot of a 25.0 kW propane fire as a function of fuel	
147	flow time at various compartment configurations	37
148	Fig. 25. Conditional density plot of a 25.0 kW propylene fire as a function of fuel	
149	flow time at various compartment configurations	38

150 Acknowledgments

151 The authors would like to acknowledge Christopher Brown, Marcos Fernandez, Laurean DeLauter,
152 and Michael Selepak, who aided in the collection of the experimental datasets.

153

154 **1. Introduction**

155 Backdrafts are a severe fire phenomenon that poses a life-threatening risk to anyone who
156 may encounter them. A backdraft occurs in an isolated heated enclosure starved of oxygen
157 with a substantial concentration of unburned fuel. When an opening is suddenly introduced
158 in the enclosure, a gravity current of colder air is driven inward, mixing with the residing
159 heated fuel. In the presence of an ignition source, a localized flammable mixture can ignite,
160 deflagrate, and generate an extending flame and pressure wave through the enclosure's
161 opening.

162 Fleishmann et al. [1] established the physical mechanisms conducive to a backdraft phe-
163 nomenon, such as the gravity current generated at the opening, turbulent mixing within
164 the enclosure, and ignition. Refs. [2–12] have expanded upon understanding the backdraft
165 phenomenon by examining the correlation between backdraft intensity and fuel type, com-
166 partment size, and vent/opening configurations. In order to resolve the subtleties in the
167 gravity current, mixing, ignition, and flame propagation, some works [13–17] have relied
168 on computational fluid dynamics (CFD) models. The primary objective of this work is
169 to provide a comprehensive dataset that better informs CFD models about physical and
170 chemical properties within an enclosure preceding a potential backdraft.

171 This report characterizes the spatial distribution of temperature and gas mixture composi-
172 tions from an experimental campaign focused on studying backdraft in a 2/5th scale com-
173 partment. Equivalence ratios and gas species measurements are recorded at various posi-
174 tions within the compartment, a portion surrounding a controlled ignition source. Here,
175 methane, propane, and propylene are the fuels of interest. Temperature measurements
176 recorded throughout the compartment are also provided.

177 **2. Description of Experiments**

178 All experiments were conducted at the National Fire Research Laboratory under a 3 MW
179 calorimeter (6 m canopy hood) [18]. Total heat release measurements conducted in the
180 canopy hood via oxygen consumption calorimetry are provided in Ref. [19]. All experi-
181 mental conditions described in this work were repeated at least twice.

182 **2.1. Compartment configuration**

183 All backdraft experiments were conducted in a reduced-scale enclosure (1.0 m x 1.0 m
184 x 1.5 m), 2/5th the dimensions of the ASTM fire test room. The enclosure's front had
185 a pneumatically operated door along a short wall with a 43.0 cm wide and 80.0 cm high
186 opening. The door opening is transformed into a window configuration by adding a 15.2 cm
187 high lip to the front entryway, forming a sill covering the lower half of the opening. Figure 1
188 provides a schematic of the compartment with the spark igniters, gas sampling probes, and
189 thermocouples positions. In this experimental series, two spark igniter positions were used

190 in either the middle or low spark position, 25.4 cm or 50.7 cm from the compartment floor,
191 respectively. Gas species measurements were obtained in the center of the compartment
192 (50.0 cm from the sidewall) using a stainless steel gas sampling line positioned at varying
193 heights from the compartment floor ranging from 90.0 cm to 22.0 cm, and lateral positions
194 spanning 37.5 cm and 111.0 cm from the opening of the compartment.

195 Temperature measurements were obtained from two thermocouple arrays on opposing sides
196 of the compartment. The first thermocouple array used 49.5 cm long Type K thermocouples
197 configured in a square orientation on the left wall facing the door. The second thermocou-
198 ple array comprised of four 24.8 cm long Type K thermocouples configured in a line on
199 the right wall facing the door spaced approximately 19.9 cm apart. All temperature mea-
200 surements were sampled at 1.0 Hz using a data acquisition system (DAQ) for most of the
201 experiment except for a 60 s time-interval, 20 s prior, and 40 s after an anticipated backdraft,
202 in which the sampling rate increased to 25.0 Hz. The uncertainty analysis for temperature
203 measurements is described in Appendix A.1.

204 Gaseous fuels were fed into a 17.8 cm square sand burner whose center was approximately
205 1.25 m from the front opening of the compartment. In some instances, a boroscope was
206 implemented to observe the flame structure at the burner while the compartment remained
207 closed. A 3.8 cm diameter vent was constructed in the lower right wall of the compartment,
208 38.0 cm from the front interior wall of the compartment and 3.0 cm above the compartment
209 floor. The vent's purpose was to prevent overpressure within the compartment by allowing
210 a uniform leakage area when the door is closed. A detailed description of the compartment
211 is available in Ref. [20].

212 2.2. Experimental procedure

213 Backdraft experiments were initiated when a small sand burner, fed fuel via mass flow
214 controller, was ignited using a propane wand ($t=0$). Initially, the fire burned while the
215 compartment doorway remained open for 60 s ($t=60$). After the front doorway was closed,
216 fuel continued to be fed into the sand burner until a predetermined fuel flow time was
217 achieved. The doorway remained closed for an additional 30 s, after which the doorway
218 opened, and a potential backdraft was observed.

219 Backdraft measurements were obtained using either methane, propane, or propylene as
220 a fuel source. Methane fire sizes included 25.0 kW, 31.3 kW, and 37.5 kW. Propane
221 fire sizes included 16.7 kW, 20.9 kW, and 25.0 kW. Propylene fire sizes only include
222 $25.0 \text{ kW} \pm 1.0 \text{ kW}$. Fuel flow times were adjusted following fire size. A list of fuel flow
223 times for each fire configuration is provided in Table 1. The uncertainty for all fire sizes
224 was approximately 1.0 kW.

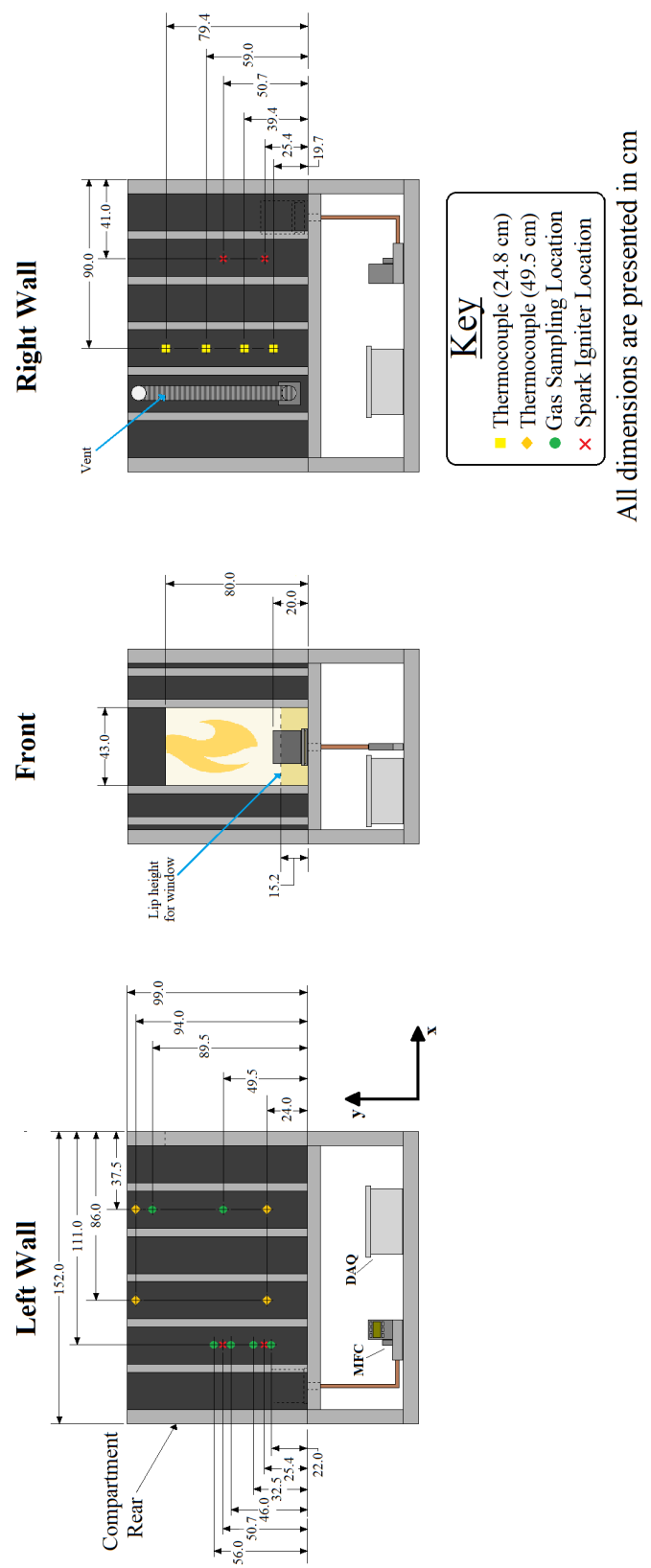


Fig. 1. Schematic of the 2/5th scale compartment utilized for backdraft experiments.

Table 1. List of fuel flow times for each fire configuration

Fuel	Fire size (kW)	Fuel flow time (s)
Methane	25.0 ± 1.0 kW	360, 390, 420, 450
	31.3 ± 1.0 kW	300, 360
	37.5 ± 1.0 kW	240, 270, 285, 300
Propane	16.7 ± 1.0 kW	270, 300, 315, 330
	20.9 ± 1.0 kW	210, 225, 240, 285
	25.0 ± 1.0 kW	240, 270, 285, 300
Propylene	25.0 ± 1.0 kW	210, 240, 270

225 **2.3. Gas composition measurements**

226 Measurements of gas mixture compositions were examined at two locations within the
227 compartment for each backdraft experiment. Each sampling position was located approx-
228 imately $50.0 \text{ cm} \pm 2.0 \text{ cm}$ from the sidewall of the compartment. In total, three sets of
229 different locations were selected as positions of interest:

- 230 1. In the upper ($y=94.0 \text{ cm}$) and middle ($y=49.5 \text{ cm}$) layer of the compartment
231 2. Approximately 5.0 cm above ($y=56.0 \text{ cm}$) and below ($y=46.0 \text{ cm}$) the middle spark
232 igniter ($y=50.7 \text{ cm}$)
233 3. Approximately 7.0 cm above ($y=32.5 \text{ cm}$) and 3.0 cm below ($y=22.0 \text{ cm}$) the low
234 spark igniter ($y=25.4 \text{ cm}$)

235 In experiments where gas samples were extracted around a spark igniter, the igniter of
236 interest was the only source of ignition.

237 Extracted gas samples were portioned into a gas analyzer, a 300 ml stainless steel reservoir
238 fitted with baffles, and a phi meter at all locations. The gas analyzer included a param-
239 agnetic and two non-dispersive infrared sensors to provide real-time oxygen, O_2 , carbon
240 dioxide, CO_2 , and carbon monoxide, CO, concentration measurements. A chiller, fitted
241 with a large volume particulate filter at its inlet, was positioned upstream of the gas ana-
242 lyzer to prevent water vapor and soot from compromising the analyzer. Therefore, all O_2 ,
243 CO_2 , and CO concentration measurements were obtained on a dry basis. A description of
244 the uncertainty analysis for O_2 , CO_2 , and CO concentration measurements obtained from
245 the gas analyzer is described in Appendix A.2.

246 The stainless-steel reservoir was used to collect well-mixed gas samples that an Agilent
247 5977E Series Gas Chromatograph analyzed with thermal conductivity and mass selectivity
248 detectors (GC/MSD). The GC/MSD analysis provided time-averaged gas species concen-
249 trations of combustion products using a method described in Refs. [21, 22]. Gas samples
250 were extracted through a sampling line via a vacuum pump for a 1 min period, initiated
251 70 s before the door opened. Time-averaged species concentration measurements were es-
252 timated to represent an extracted gas mixture obtained 20 s prior to the door opening. A

253 detailed description of the uncertainty analysis of time-averaged gas species measurements
 254 obtained via GC/MSD is reported in Ref. [21].

255 A phi meter [23, 24] was implemented to evaluate the extracted gas sample's global and lo-
 256 cal equivalence ratios. Unlike other gas sampling techniques [25, 26], a phi meter provides
 257 real-time equivalence ratio measurements without knowledge of the initial fuel or com-
 258 busted gas mixture. The phi meter utilizes a high-temperature catalytic reactor to facilitate
 259 lean combustion via excess oxygen to the sampling line. The lean combustion results in
 260 an exhaust exclusively comprised of oxygen, carbon dioxide, water vapor, and inert gases.
 261 The reactor exhaust is then cooled to condense water from the gas line preserving the in-
 262 tegrity of downstream measurement devices. Downstream measurement devices include a
 263 mass flow controller, vacuum pump, and gas analyzer capable of measuring oxygen and
 264 carbon dioxide concentrations. The mass flow controller is implemented to regulate the
 265 total flow through the phi meter's reactor, driven by the vacuum pump located downstream.
 266 Before entering the pump, oxygen and carbon dioxide concentration measurements of the
 267 gas stream are recorded and used to calculate the global equivalence ratio.

268 The global equivalence ratio, ϕ_G , is calculated by the phi meter's O₂ and CO₂ concentra-
 269 tion measurements in the dried reactor's exhaust stream, X_{O₂} and X_{CO₂}, and the mass flow
 270 controller volumetric flow, \dot{V}_{MFC} , measurements in the equation below, where X_{O_{2,Ent}} is the
 271 concentration of oxygen in the air (approx. 20.95%) and $\dot{V}_{O_2,Ex}$ is the volumetric flows of
 272 the excess oxygen, respectively.

$$\phi_G = 1 + \left(\frac{1 - X_{O_2,Ent}}{X_{O_2,Ent}(1 - X_{O_2} - X_{CO_2})} \right) \left(\frac{\dot{V}_{O_2,Ex}}{\dot{V}_{MFC}} - X_{O_2,A} \right) \quad (1)$$

273 The local equivalence ratio, ϕ_L , is estimated from the phi meter by determining the oxygen
 274 consumption for the lean combustion in the reactor, as defined in the equation below.

$$\phi_L = 1 + \frac{\dot{m}_{O_2,Ex.} - \dot{m}_{O_2,O}}{\dot{m}_{O_2,Samp.}} \quad (2)$$

275 Here, $\dot{m}_{O_2,Ex.}$ is the mass flow of excess oxygen introduced at the inlet of the phi meter,
 276 $\dot{m}_{O_2,O}$ is the mass flow of oxygen measured at the outlet of the phi meter's reactor, and
 277 $\dot{m}_{O_2,Samp.}$ is the mass flow of oxygen in the extracted sample at the inlet of the phi me-
 278 ter. The oxygen concentration in the extracted sample is estimated from O₂ measurements
 279 provided by the external paramagnetic sensor. A full derivation of Eq. 2 is provided in
 280 Ref. [24]. Uncertainty analyses of the phi meter's global and local equivalence ratio mea-
 281 surements is given in Appendix A.3 and A.4, respectively.

282 Sample lines feeding into the phi meter and stainless-steel reservoir were heated (approx.
 283 90 °C ± 5 °C) using heating tape eliminating water vapor condensation in the extracted
 284 sample. Gas species concentrations in the paramagnetic sensor and phi meter data were
 285 recorded at 1 Hz throughout the experiment using a DAQ.

286 **3. Results**

287 This section presents real-time and averaged temperature and gas mixture composition
288 measurements taken at different positions within the enclosure before an anticipated back-
289 draft.

290 **3.1. Temperature measurements**

291 **3.1.1. Real-Time temperature measurements**

292 Figure 2 presents the real-time temperature measurements from both thermocouple arrays
293 of the 25.0 kW, 31.3 kW, and 37.5 kW methane fires subjected to different fuel flow times.
294 The temperature steadily increased for each methane fire configuration until the flame struc-
295 ture diminished, causing the temperature to peak and then decline. The diminishing flame
296 structure was confirmed via boroscope observation. When a backdraft occurs, temperatures
297 at all positions within the compartment spike, then rapidly decline. No spike was observed
298 in instances where a backdraft did not occur, and the temperature declined steadily.

299 The temperature data measured on the left wall of the enclosure demonstrates that temper-
300 atures were higher in the upper region and back of the compartment, farther away from the
301 doorway and vent. The right wall temperature profiles further demonstrate the temperature
302 gradient as a function of height, wherein temperatures were higher farther up within the
303 compartment. The initial temperature climb prior to the flame diminishing is observed to
304 increase faster with fire size at most positions within the enclosure.

305 Experiments utilizing propane fires are shown to echo similar temperature profiles as that
306 of experiments with methane fires and are displayed in Fig. 3. Here, real-time tempera-
307 ture measurements from both thermocouple arrays of the 16.7 kW, 20.9 kW, and 25.0 kW
308 propane fires subjected to different fuel flow times are shown. Temperatures were higher
309 at locations farther up and back within the compartment. Initial temperature ramps and
310 peaks are shown to increase with propane fire size. In comparison to an experiment utiliz-
311 ing a 25.0 kW methane fire, the 25.0 kW propane fire size demonstrates higher temperature
312 profiles at most positions.

313 Figure 4 displays the temperature profiles obtained from both thermocouple arrays for a
314 25.0 kW propylene fire with a fuel flow time of 270 s. Similar temperature profiles are
315 exhibited. Compared to the temperature profiles in experiments with a 25.0 kW propane
316 fire size, the initial peak temperature is lower and less distinguishable on the left wall.

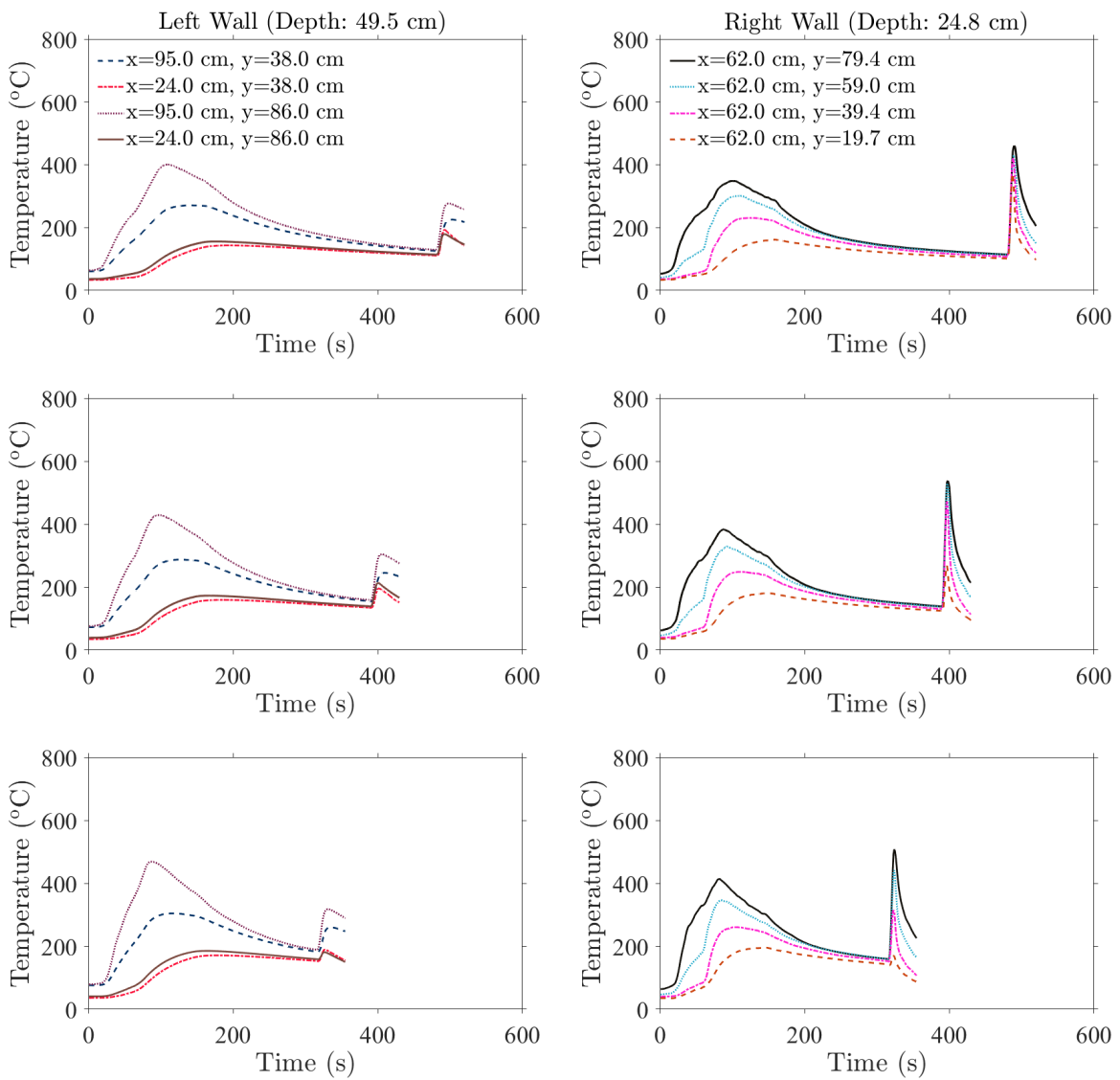


Fig. 2. Real-time temperature measurements of the 25.0 kW methane fire with a fuel flow time of 450 s (top), the 31.3 kW methane fire with a fuel flow time of 360 s (middle), and the 37.5 kW methane fire with a fuel flow time of 285 s (bottom) at different positions within the compartment. The expanded uncertainty of the temperature measurement estimated from the Type B evaluation of standard uncertainty is approximately 2.20 $^{\circ}\text{C}$ or 0.75% of the reading, whichever is greater.

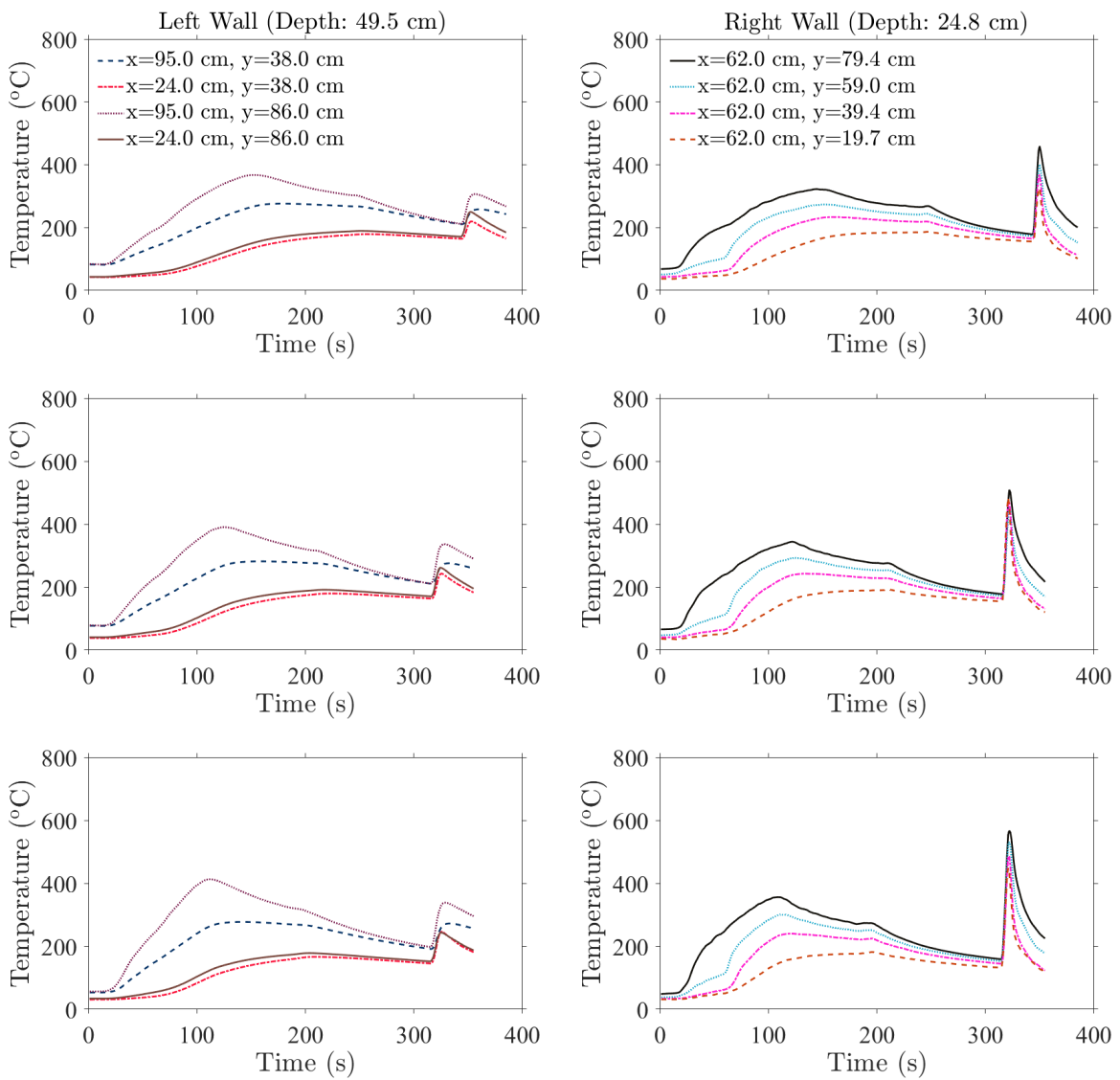


Fig. 3. Real-time temperature measurements of the 16.7 kW propane fire with a fuel flow time of 315 s (top), the 20.9 kW propane fire with a fuel flow time of 285 s (middle), and the 25.0 kW propane fire with a fuel flow time of 285 s (bottom) at different positions within the compartment. The expanded uncertainty of the temperature measurement estimated from the Type B evaluation of standard uncertainty is approximately 2.20 °C or 0.75% of the reading, whichever is greater.

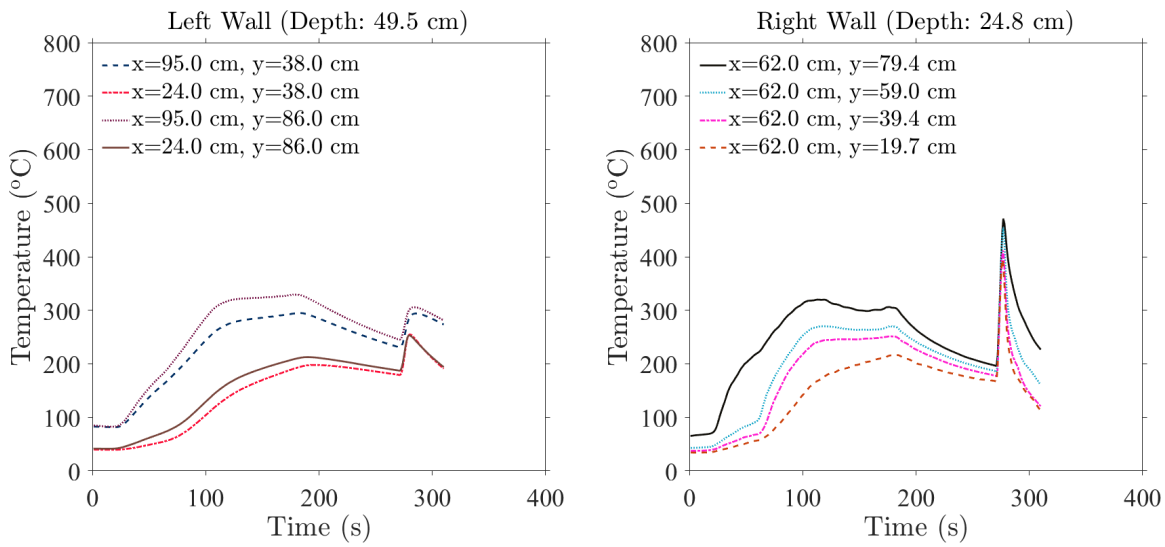


Fig. 4. Real-time temperature measurements of a 25.0 kW propylene fire with a fuel flow time of 270 s at different positions within the compartment. The expanded uncertainty of the temperature measurement estimated from the Type B evaluation of standard uncertainty is approximately 2.20 °C or 0.75% of the reading, whichever is greater.

317 **3.1.2. Time-Averaged temperature measurements**

318 Time-Averaged temperature measurements are presented in Figs. 5, 6, and 7 for experiments
319 utilizing methane, propane, and propylene, respectively, at different fire sizes and
320 fuel flow times. Time-average measurements were estimated from the mean averaged tem-
321 perature measurements in repeated experiments subjected to the same conditions. Each
322 experiment determined averaged temperature measurements from readings recorded 10 s
323 prior to the doorway opening. The uncertainty of the time-averaged temperature mea-
324 surements was estimated from a combined Type A and Type B evaluations of standard
325 uncertainty, as detailed in Appendix B.

326 Compared to the real-time data shown in Figs. 2, 3, and 4, the time-averaged data for the
327 methane, propane, and propylene fires follow a similar trend. The temperature decreases
328 the longer the duration from when the initial flame is extinguished. Furthermore, as the fuel
329 flow time increases, time-averaged temperatures at various positions converge to a constant
330 value suggesting a bulk fluid temperature within the compartment.

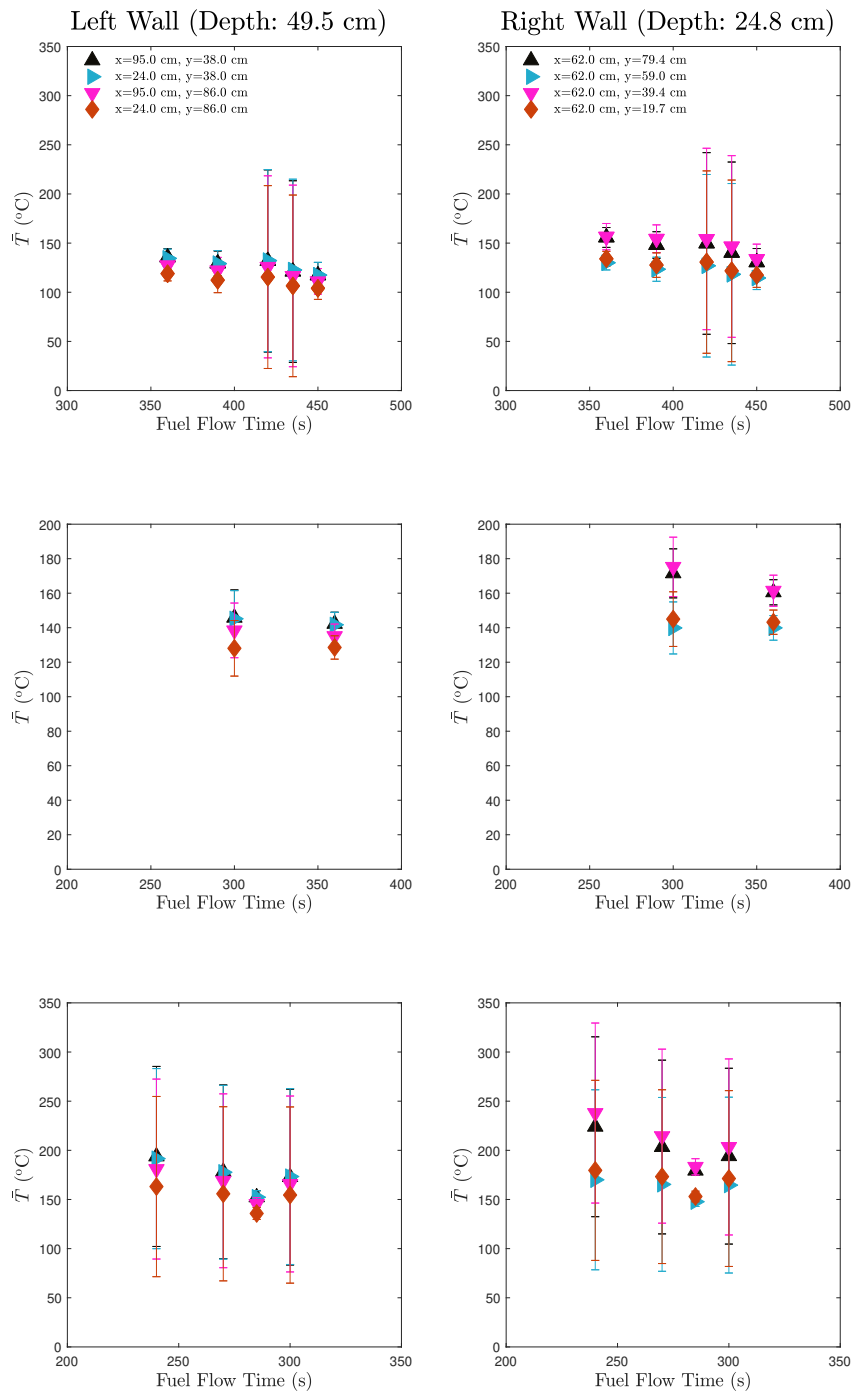


Fig. 5. Time-averaged temperature measurements of the 25.0 kW (top), 31.3 kW (middle), and 37.5 kW (bottom) methane fires with different fuel flow times at different positions within the compartment. The combined uncertainty of the time-averaged temperature measurement is estimated from a combination of the Type A and B evaluations of standard uncertainty.

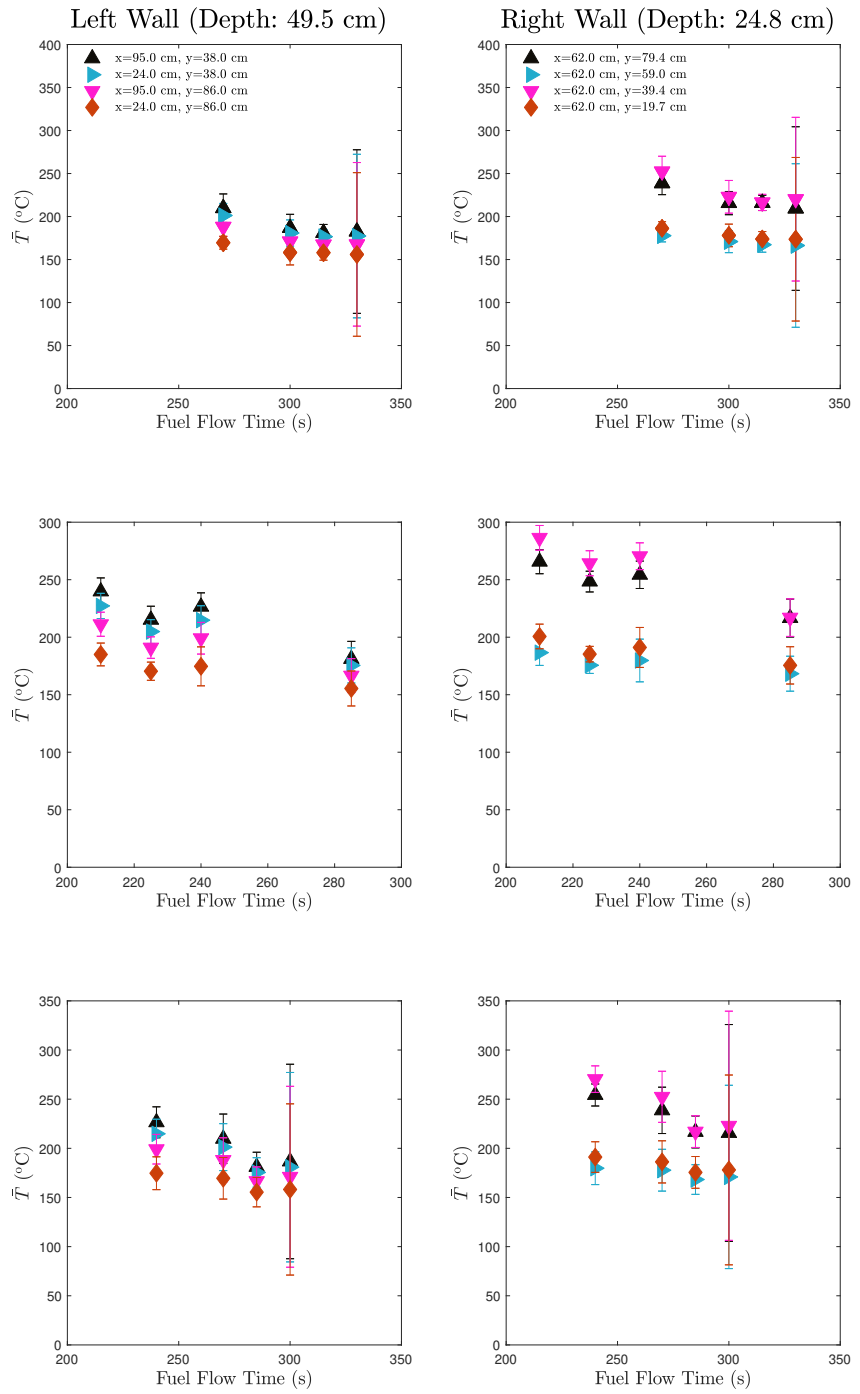


Fig. 6. Time-averaged temperature measurements of the 16.7 kW (top), 20.9 kW (middle), and 25.0 kW (bottom) propane fires with different fuel flow times at different positions within the compartment. The combined uncertainty of the time-averaged temperature measurement is estimated from a combination of the Type A and B evaluations of standard uncertainty.

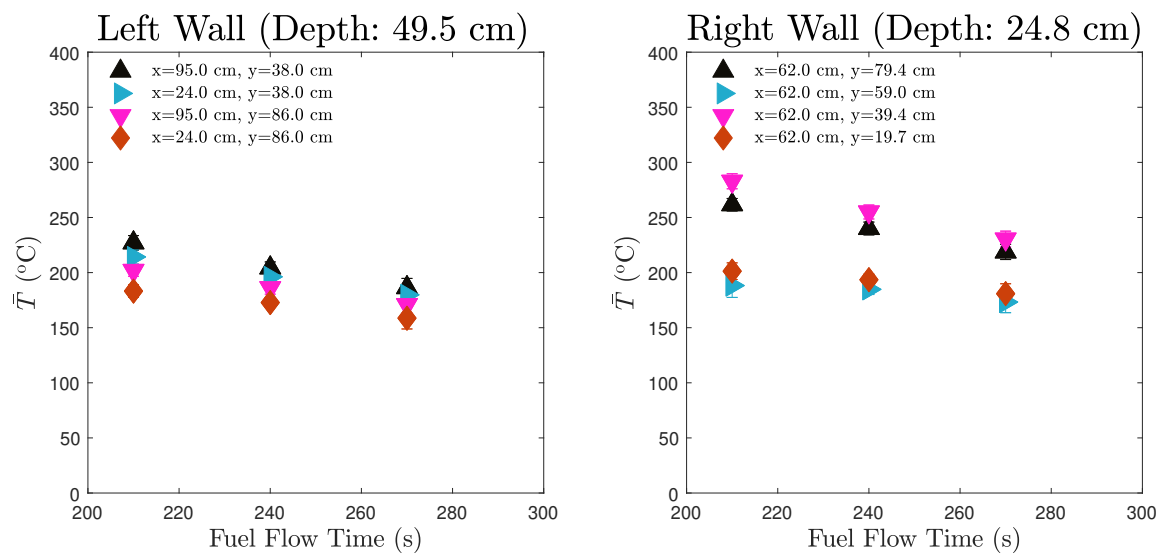


Fig. 7. Time-averaged temperature measurements of the 25.0 kW propylene fire with different fuel flow times at different positions within the compartment. The combined uncertainty of the time-averaged temperature measurement is estimated from a combination of the Type A and B evaluations of standard uncertainty.

331 **3.2. Gas mixture composition measurements**

332 **3.2.1. Real-Time gas mixture composition measurements**

333 Real-time gas mixture composition measurements are presented in Fig. 8 for a 25.0 kW,
334 31.3 kW, and 37.5 kW methane fire with various fuel flow times and at different positions
335 within the compartment. Gas mixture composition measurements include the global and
336 local equivalence ratios and gas concentrations of O₂, CO₂, and CO. Gas measurements
337 were obtained at two positions for each experiment, indicating that Fig. 8 is a compilation
338 of three experiments under the same condition but with different points of interest.

339 For different methane fire sizes, the gas mixture composition measurements follow a sim-
340 ilar trend. Initially, after ignition (t=0 s), the global and local equivalence ratios are close
341 to 0 at all positions as the doorway remains open. As the fire continues to burn in a qui-
342 escent environment, smoke is continuously building its presence in the upper region of the
343 compartment, attributing to the rate of decline in O₂ and increase in CO₂ and CO concen-
344 trations. As the doorway shuts (t=60 s), the oxygen declining rate cascades as a function
345 of height while the global and local equivalence ratio begins to increase, signifying the
346 growing concentration of unburned fuel, carbon dioxide, and carbon monoxide throughout
347 the compartment.

348 As the compartment remains isolated, the local equivalence ratio increases faster than the
349 global equivalence ratio, indicating an accelerated presence of unburned fuel. As discussed
350 in Ref [24], the global equivalence ratio is defined by the ratio of the sum of unburned
351 and burned fuel to the sum of unburned and burned oxygen. The local equivalence ratio
352 is defined by the ratio of only unburned fuel and oxygen. The rapid increase in the local
353 equivalence ratio compared to the slow climb of the global equivalence ratio suggests an
354 increasing presence of unburned fuel within the compartment that outpaces the carbon
355 dioxide and carbon monoxide generation from the fire.

356 For all fire configurations, at approximately 200 s ± 20 s, the flame extinguishes as ob-
357 served via boroscope. The extinguished flame may attribute to the gas mixture near the
358 burner falling below the limiting oxygen concentration for methane in the presence of
359 combustion products, approximately 14.5% ± 1% [27]. Oxygen concentration values at
360 the lowest sampling height drop below the limiting oxygen concentration at approximately
361 the same time the flame extinguishes.

362 The absence of a flame, while methane continues to flow into the compartment, increases
363 the global and local equivalence ratio's growth rate while staggering the generation of car-
364 bon dioxide and carbon monoxide. Oxygen concentrations are observed to briefly increase,
365 caused by minor ventilation in the compartment's vent and creases. When the fuel stops
366 flowing into the compartment 30 s prior to the doorway opening, the gas mixture composi-
367 tion measurements are nominally equivalent, except for the leaner mixtures observed close
368 to the compartment floor (y< 30.0 cm).

369 Upon the doorway opening, the equivalence ratios are observed to decline rapidly. At
370 lower positions within the compartment, the rapid drop in the equivalence ratios is observed
371 sooner, suggesting that the gravity current penetrates the lower region of the compartment
372 as it reaches its rear, then mixes upward. A series of images depicting the flame propagation
373 once the door opens of experiments subjected to 25 kW methane, propane, and propylene
374 fires at different fuel flow times are shown in Fig. 9. For experiments involving methane,
375 backdrafts were observed to propagate in the compartment's upper region, which further
376 supports the sudden drop of oxygen at the highest sampling position ($y=90.0$ cm).

377 Notable differences are observed between gas mixture composition measurements for dif-
378 ferent methane fire sizes. The increase in the global and local equivalence ratio is found to
379 be faster with fire size. Higher equivalence ratios and gas concentration peaks are observed
380 in experiments with larger methane fire sizes.

381 As shown in Fig. 10, experiments that utilized propane at different fire sizes displayed a
382 similar trend to methane fires before the fire extinguishing. Once the propane flame is ex-
383 tinguished, the local equivalence ratio increases faster in the compartment's middle layer
384 ($y=49.5$ cm) and closer to the front of the compartment ($x=37.5$ cm). The higher local
385 equivalence ratio in the middle layer of the compartment ($y\sim 50.0$ cm), closer to the door-
386 way, could attribute to the low concentration of oxygen in the region, which is occupied by
387 combustion products, as shown in the high carbon dioxide and carbon monoxide concen-
388 trations at the same position.

389 As the propane flow is shut off, a richer local equivalence ratio is measured closer to the
390 compartment floor ($y<30.0$ cm), indicating unburned fuel descending lower within the com-
391 partment. When the doorway opens, the local equivalence ratio is observed to spike at gas
392 sampling positions lower in the compartment. The richer mixture residing in the bottom re-
393 gion of the compartment suggests that more fuel is present when the gravity current mixes
394 into the enclosure resulting in flame propagating throughout the compartment as opposed
395 to the upper region as observed in experiments involving methane. The larger span of
396 the propane flame is demonstrated Fig. 9 which shows the flame growth throughout the
397 compartment at lower regions in the compartment relative to the methane fire experiments.

398 At the compartment's lowest sampling position ($y=22.0$ cm), the global and local equiva-
399 lence ratio peaks increase with propane fire size. The local equivalence ratio at the middle
400 sampling position ($y=49.5$ cm), closer to the doorway ($x=37.5$ cm), is shown to peak with
401 increasing fire size at the approximate time the initial flame is extinguished. Carbon monox-
402 ide concentrations are also found to peak close to the compartment floor ($y<35.0$ cm) during
403 a backdraft, further supporting the fuel-rich mixture in the lower layer of the compartment
404 when the doorway opens.

405 Gas mixture composition measurements obtained in experiments utilizing a 25 kW propy-
406 lenes fire were only taken at two sampling locations. The limited dataset is presented in
407 Fig. 11. Measurement profiles of the 25 kW propylene fire were observed to follow similar
408 trends to that of experiments involving the 25 kW propane fire. Equivalence ratios were

⁴⁰⁹ higher at the lower sampling position, indicating a richer mixture close to the compartment
⁴¹⁰ floor when the doorway opens. The local phi and carbon monoxide concentrations peak
⁴¹¹ during a backdraft, suggesting a richer fuel mixture as the gravity current flows into the
⁴¹² enclosure. As the doorway opens, the rich lower region is further made evident through vi-
⁴¹³ sual observation of flame geometry, which propagated throughout the compartment during
⁴¹⁴ a backdraft, as shown in Fig. 9.

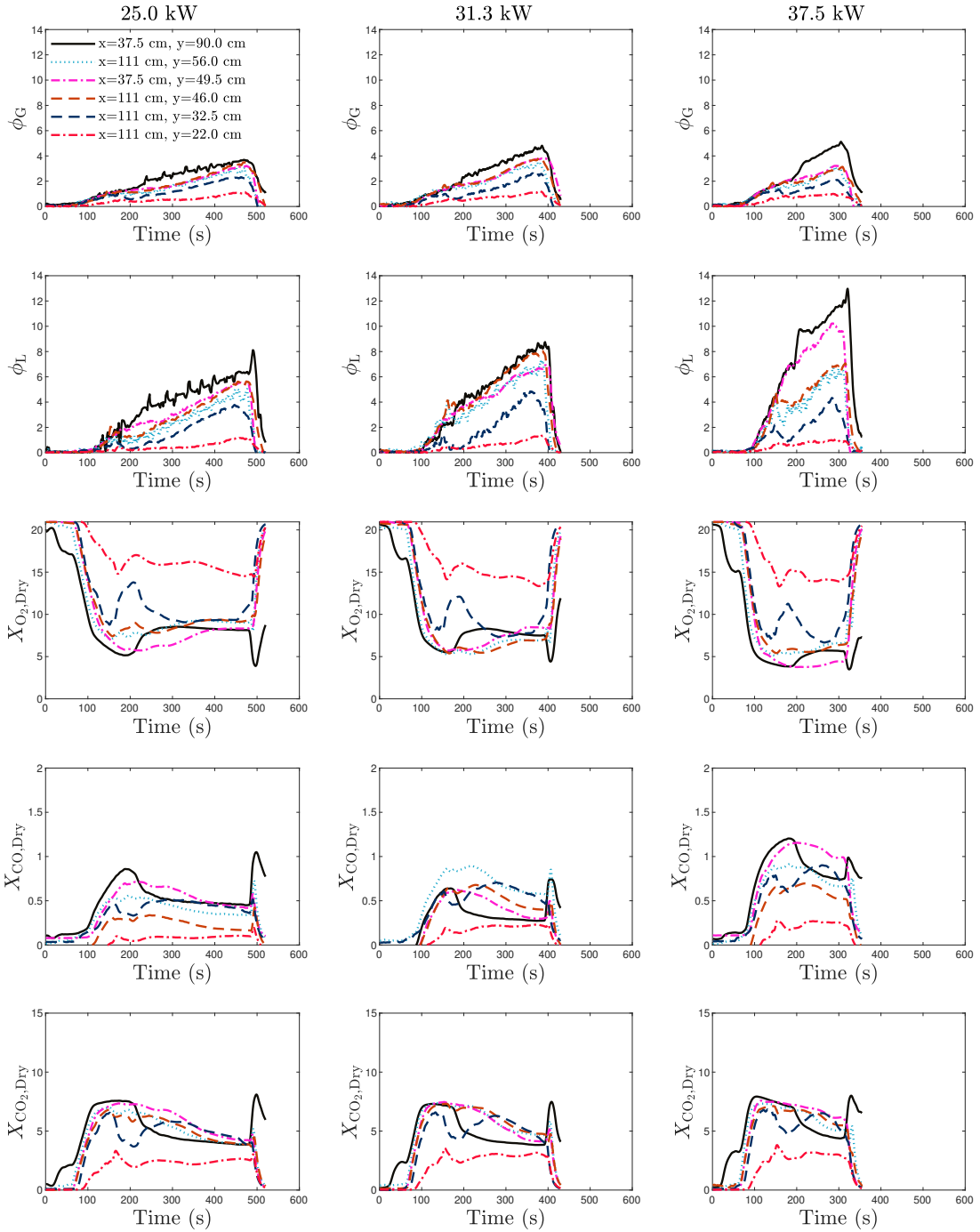


Fig. 8. Real-time gas mixture composition measurements of the 25.0 kW methane fire with a fuel flow time of 450 s (left), the 31.3 kW methane fire with a fuel flow time of 360 s (center), and the 37.5 kW methane fire with a fuel flow time of 285 s (right) at different positions within the compartment. The uncertainty of the gas mixture composition measurements is described in Appendix A.

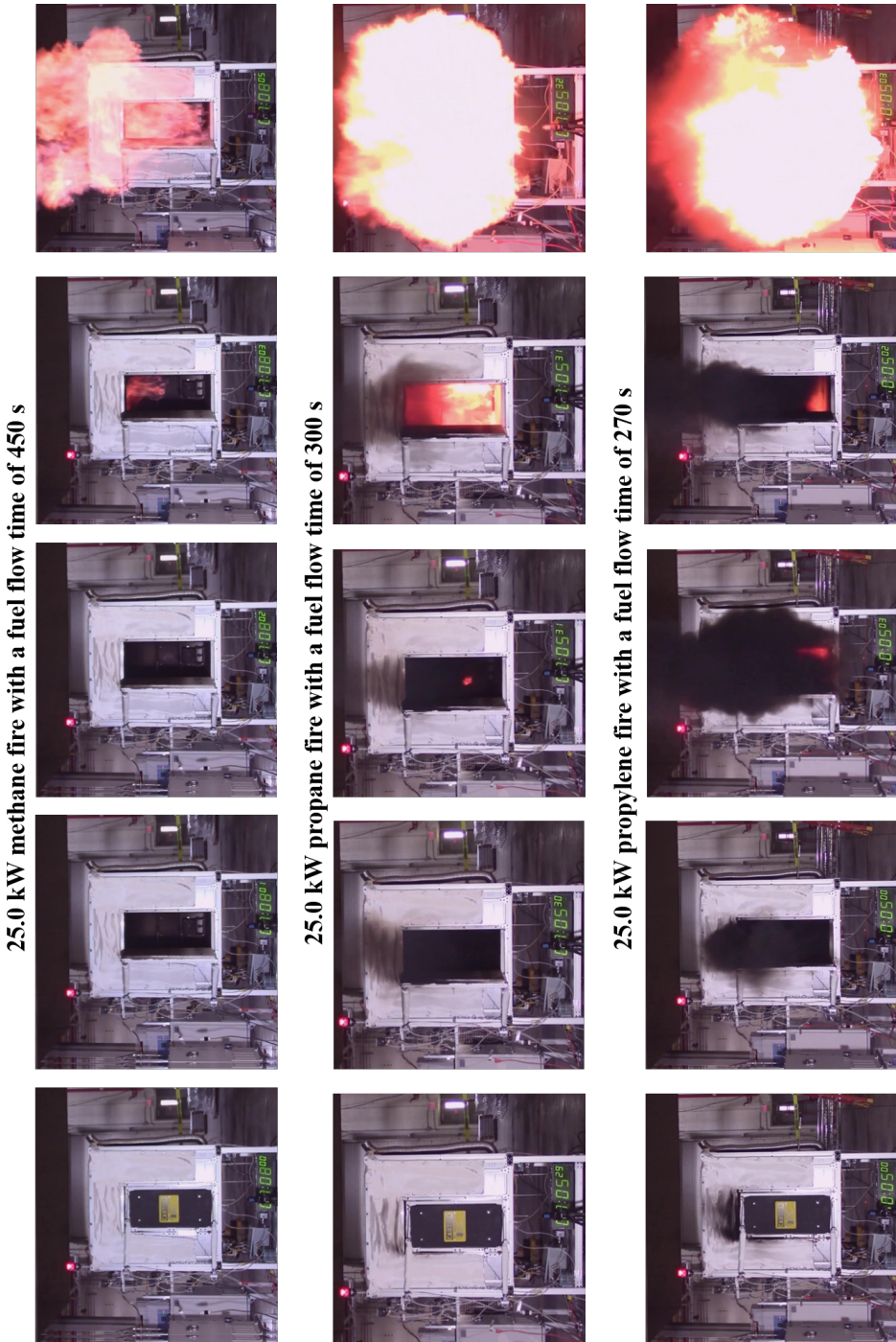


Fig. 9. Sequences of flame propagation in the compartment previously subjected to 25.0 kW methane, propane, and propylene fires with a fuel flow time of 450 s, 300 s, and 270 s, respectively. For each presented experiment, the compartment is configured with a low spark igniter position.

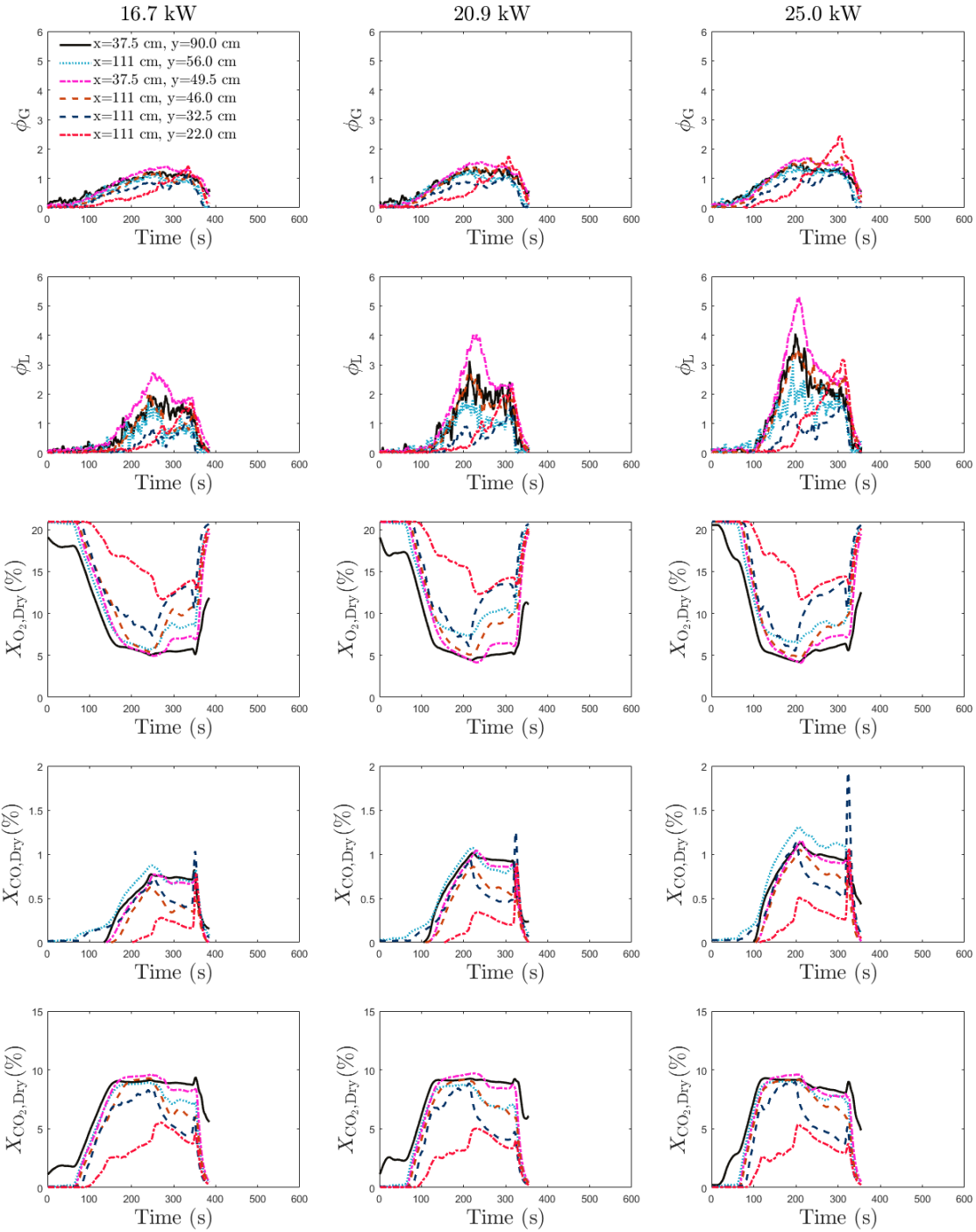


Fig. 10. Real-time gas mixture composition measurements of the 16.7 kW propane fire with a fuel flow time of 315 s (left), the 20.9 kW propane fire with a fuel flow time of 285 s (center), and the 25.0 kW propane fire with a fuel flow time of 285 s (right) at different positions within the compartment. The uncertainty of the gas mixture composition measurements is described in Appendix A.

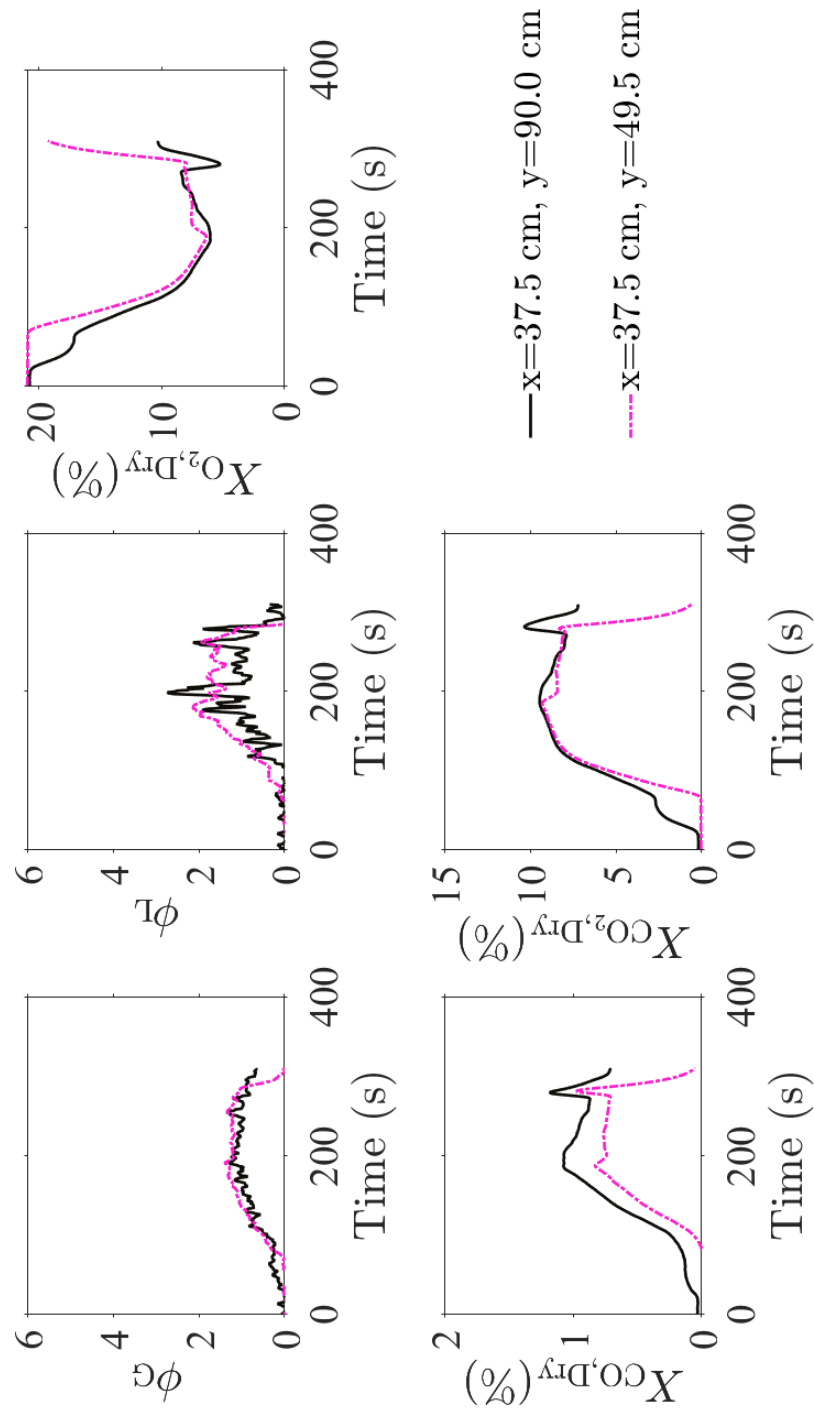


Fig. 11. Real-time gas mixture composition measurements of a 25.0 kW propylene fire with a fuel flow time of 270 s at different positions within the compartment. The uncertainty of the gas mixture composition measurements is described in Appendix A.

415 **3.2.2. Time-Averaged gas mixture composition measurements**

416 Figures 12, 13, and 14 display the time-averaged gas mixture composition measurements
417 for experiments utilizing methane, propane, and propylene fires, respectively, of different
418 sizes and fuel flow times. Time-average measurements were estimated from the mean av-
419 eraged gas mixture composition measurements made in repeated experiments subjected to
420 the same conditions. Each experiment determined averaged gas mixture composition mea-
421 surements from readings recorded 10 s prior to the doorway opening. The uncertainty of the
422 time-average gas mixture composition measurements was estimated from a combined Type
423 A and B evaluations of standard uncertainty. Further details are described in Appendix B.

424 When presented as a function of fuel flow time, the time-averaged gas mixture composi-
425 tion measurements mimic trends displayed in Figs. 8, 10, 11. The global and local equiva-
426 lence ratios increase with fuel flow time in instances where the parent fuel is methane.
427 The local equivalence ratio is nominally consistent in the middle region of the compart-
428 ment ($y \sim 50.0$ cm) for most configurations. Time-averaged oxygen concentrations at the
429 lowest sampling position are approximately $15\% \pm 0.5\%$ for all fire sizes and fuel flow
430 times. Time-averaged carbon monoxide and carbon dioxide concentration measurements
431 are nominally consistent in the upper region of the compartment ($y > 50$ cm) regardless of
432 fuel flow time and are observed to increase with fire size.

433 Time-averaged gas mixture composition measurements for experiments involving propane
434 fires at various fuel flow times are shown in Fig. 13. Compared to methane experiments,
435 the time-averaged global and local equivalence ratio measurements obtained in experiments
436 with propane fires are lower and are observed to converge to an approximate value at the
437 fuel flow time increase. Oxygen concentration is also observed to be higher closer to the
438 compartment floor. Carbon dioxide and carbon monoxide measurements are shown to
439 reiterate observations from Fig. 10 in that the concentrations remain relatively constant in
440 the upper region of the compartment ($y > 50.0$ cm) but a decline in the lower region as the
441 fuel flow time increase.

442 Figure 14 presents the time-averaged gas mixture composition measurements at two sam-
443 pling locations for experiments utilizing a 25 kW propylene fire. Similar to propane exper-
444 iments, the relationship between the gas mixture composition measurement and fuel flow
445 time is similar. The difference between equivalence ratio measurements decreases with an
446 increase in fuel flow time. Carbon dioxide and carbon monoxide concentration measure-
447 ments are independent of fuel flow time.

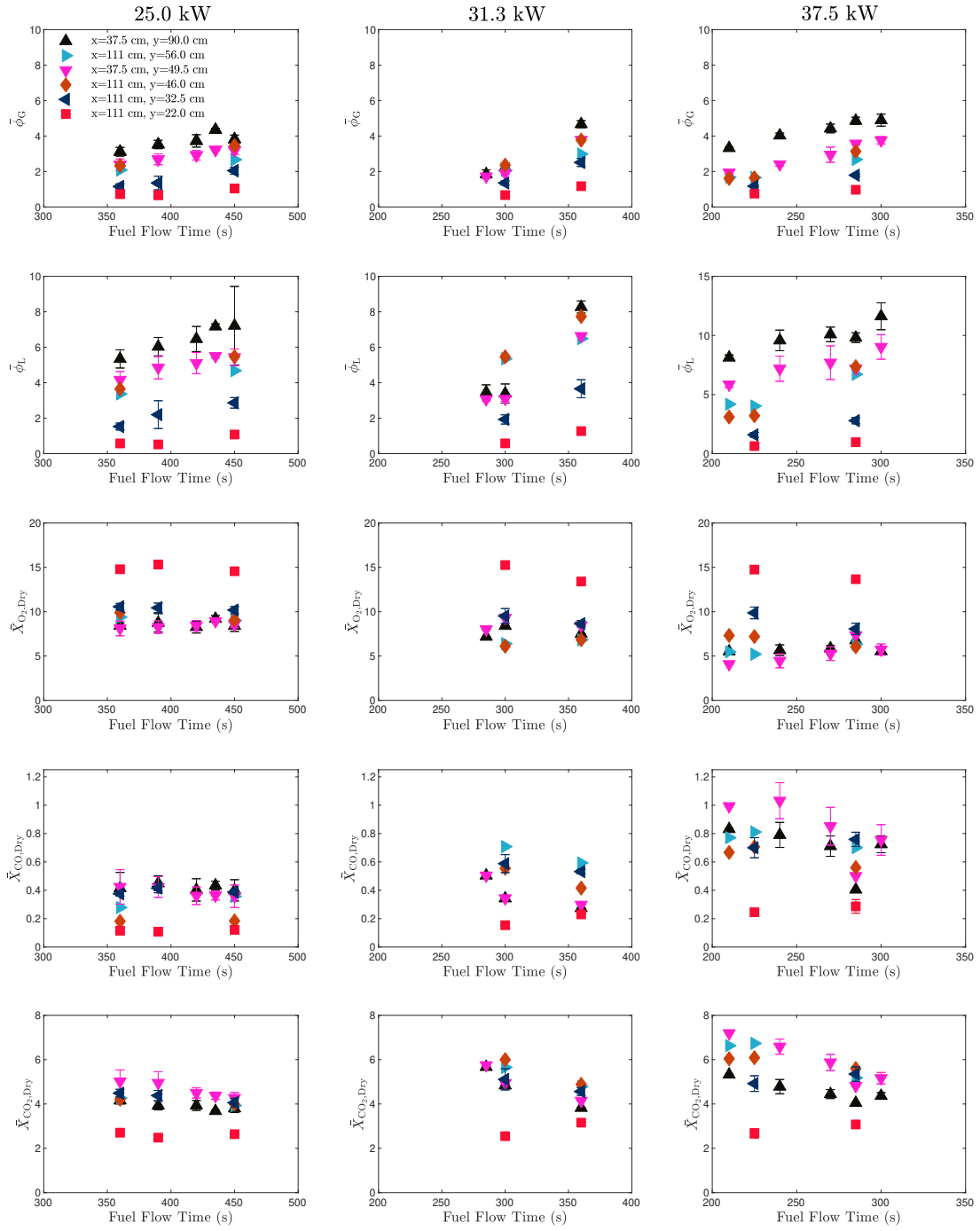


Fig. 12. Time-averaged gas mixture composition measurements of the 25.0 kW, 31.3 kW, and 37.5 kW methane fires with different fuel flow times at different positions within the compartment. The time-averaged gas mixture composition's combined uncertainty is estimated from a combination of the Type A and B evaluations of standard uncertainty. Uncertainty analysis of the time-averaged gas mixture concentration measurements is provided in Appendix B.

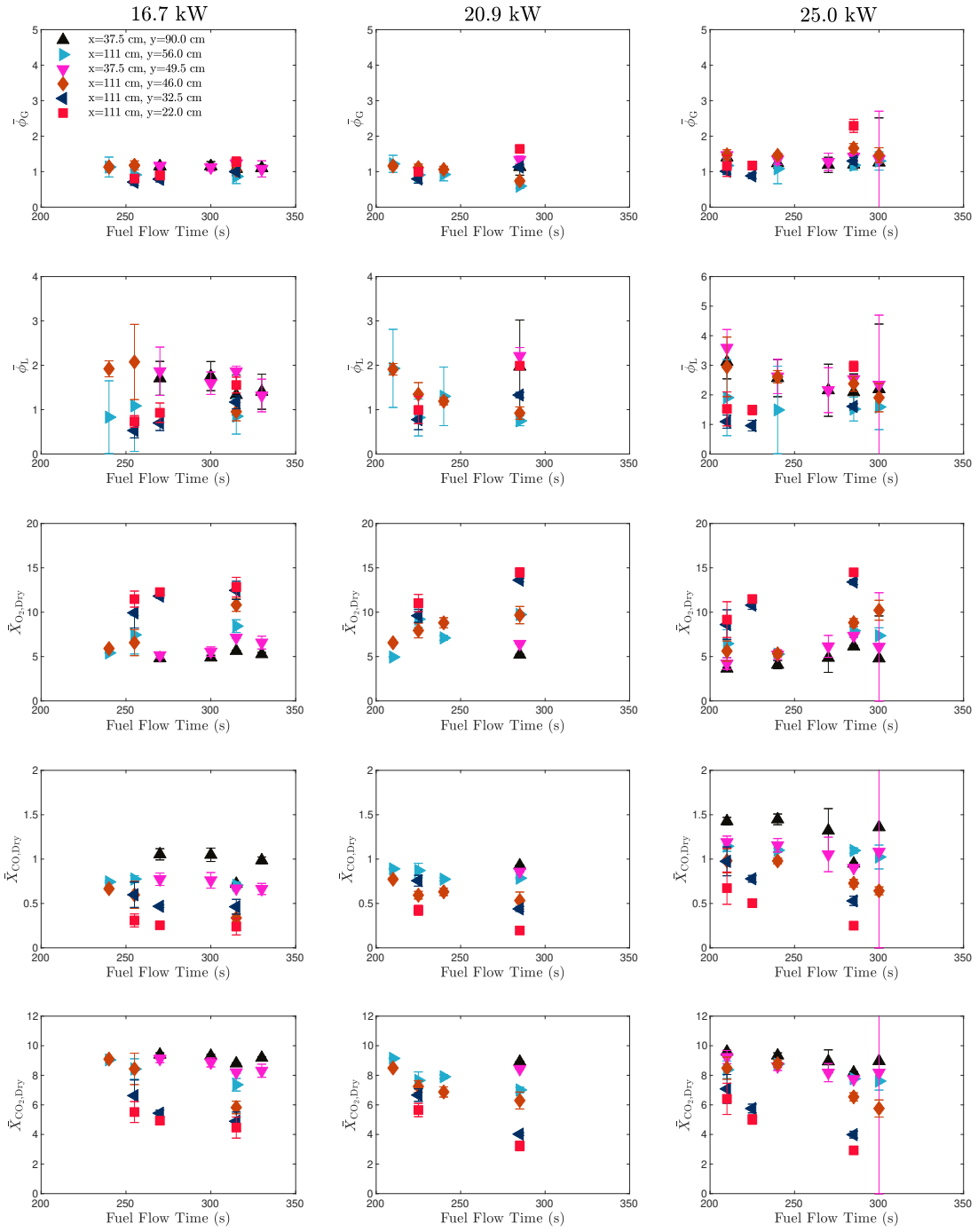


Fig. 13. Time-averaged gas mixture composition measurements of the 16.7 kW, 20.9 kW, and 25.0 kW propane fires with different fuel flow times at different positions within the compartment. The combined uncertainty of the time-averaged gas mixture composition measurements is estimated from a combination of the Type A and B evaluations of standard uncertainty. Uncertainty analysis of the time-averaged gas mixture concentration measurements is provided in Appendix B.

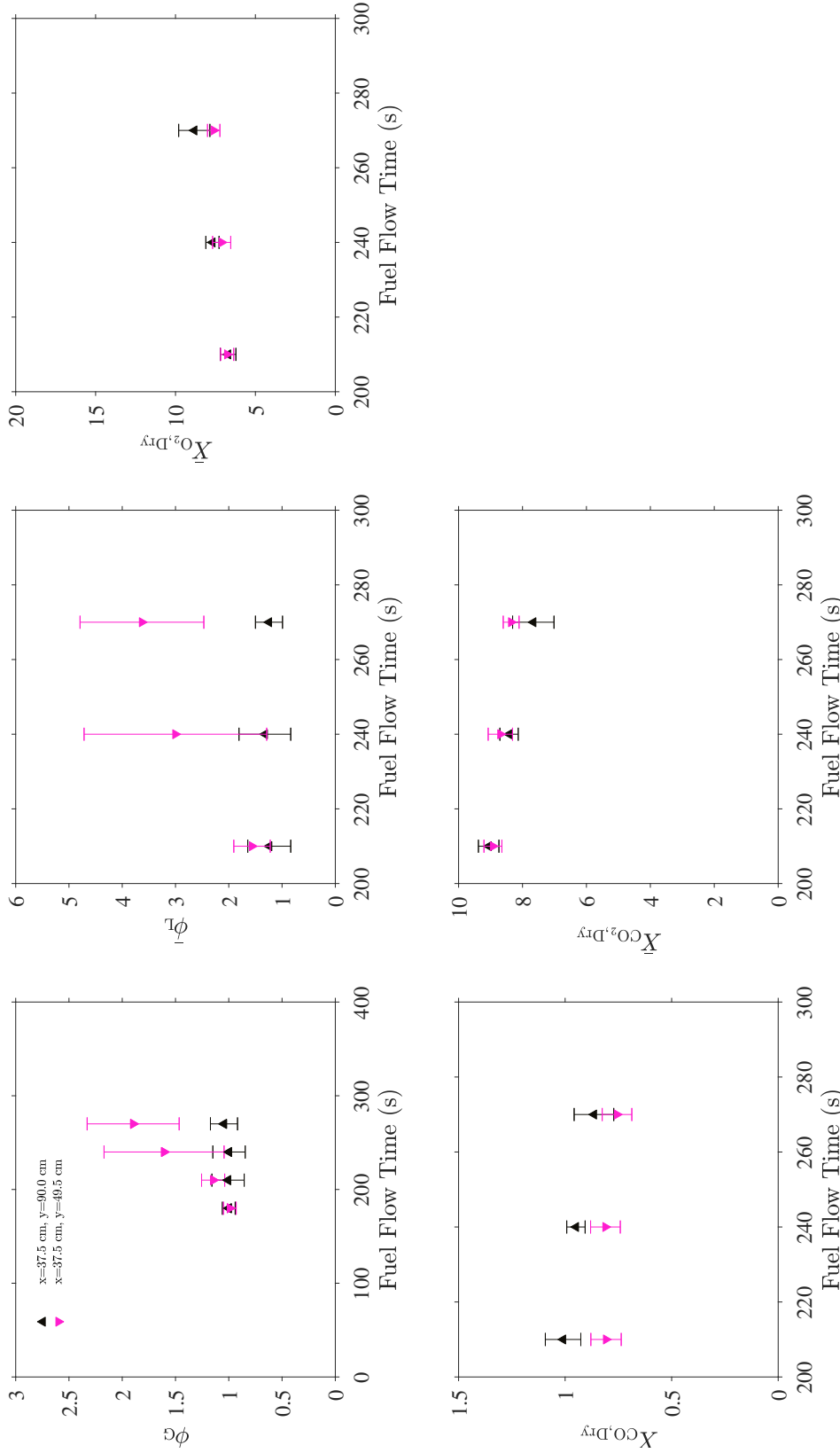


Fig. 14. Time-averaged gas mixture composition measurements of the 25.0 kW propylene fire with different fuel flow times at different positions within the compartment. The combined uncertainty of the time-averaged gas mixture composition measurements is estimated from a combination of the Type A and B evaluations of standard uncertainty. Uncertainty analysis of the time-averaged gas mixture concentration measurements is provided in Appendix B.

448 A more detailed description of the gas mixture composition is provided in the time-averaged
449 gas species concentration measurements determined via GC/MSD. The time-averaged species
450 concentration measurements are presented in Fig 15, 16, and 17 for experiments utilizing
451 methane, propane, and propylene, respectively, at different fire sizes and fuel flow times.
452 In these figures, the concentration of fuel, \bar{X}_{Fuel} , is the sum of all unburned fuel species de-
453 tected in the gas sample. In addition to the parent fuel, other unburned fuel species include
454 trace amounts of acetylene, ethylene, ethane, and benzene. Trace amounts of propylene
455 were observed in gas samples obtained from experiments involving propane as the parent
456 fuel.

457 The time-averaged gas species measurements complement phi meter and gas analyzers' measurements
458 for experiments implementing methane as the fuel source. The total fuel concentration is shown to increase at all positions as the fuel flow time increases, similar
459 to how the global and local equivalence ratios increases in Fig 8. The fuel concentration
460 is higher in the upper region of the compartment, closer to the doorway. Combustion
461 products (i.e., carbon dioxide, water vapor, and carbon monoxide) and inert (i.e., nitrogen
462 and argon) are reasonably steady as fuel flow time increases. Higher concentrations of
463 water vapor are observed in instances with high oxygen concentrations. The highest carbon
464 monoxide concentration is observed in the compartment's middle layer for every fuel flow
465 time, as demonstrated by gas analyzer measurements in Figs. 8 and 12.

466 Figure 16 presents the time-averaged gas species measurements in experiments with the
467 16.7 kW and 25.0 kW propane fires at different fuel flow times. No gas samples were
468 collected for the 20.9 kW propane fire. In both instances of different fire sizes, the fuel
469 concentration is found to be nominally constant regardless of the fuel flow time. Higher
470 oxygen concentrations were measured in the lower region of the compartment ($y < 50.0$ cm),
471 farther back from the doorway ($x = 111.0$ cm). Inversely, combustion product concentrations
472 were higher at positions where the oxygen concentrations were low. The consistent con-
473 centrations of gas species at the same position but varying fuel flow time support previously
474 described. gas mixture composition measurements.

475 Extracted gas samples to be processed by the GC/MSD were acquired at only two positions
476 for experiments with a 25 kW propylene fire. The time-averaged gas species concentrations
477 are presented in Fig. 17. Gas species concentrations are consistent at the different fuel flow
478 times.

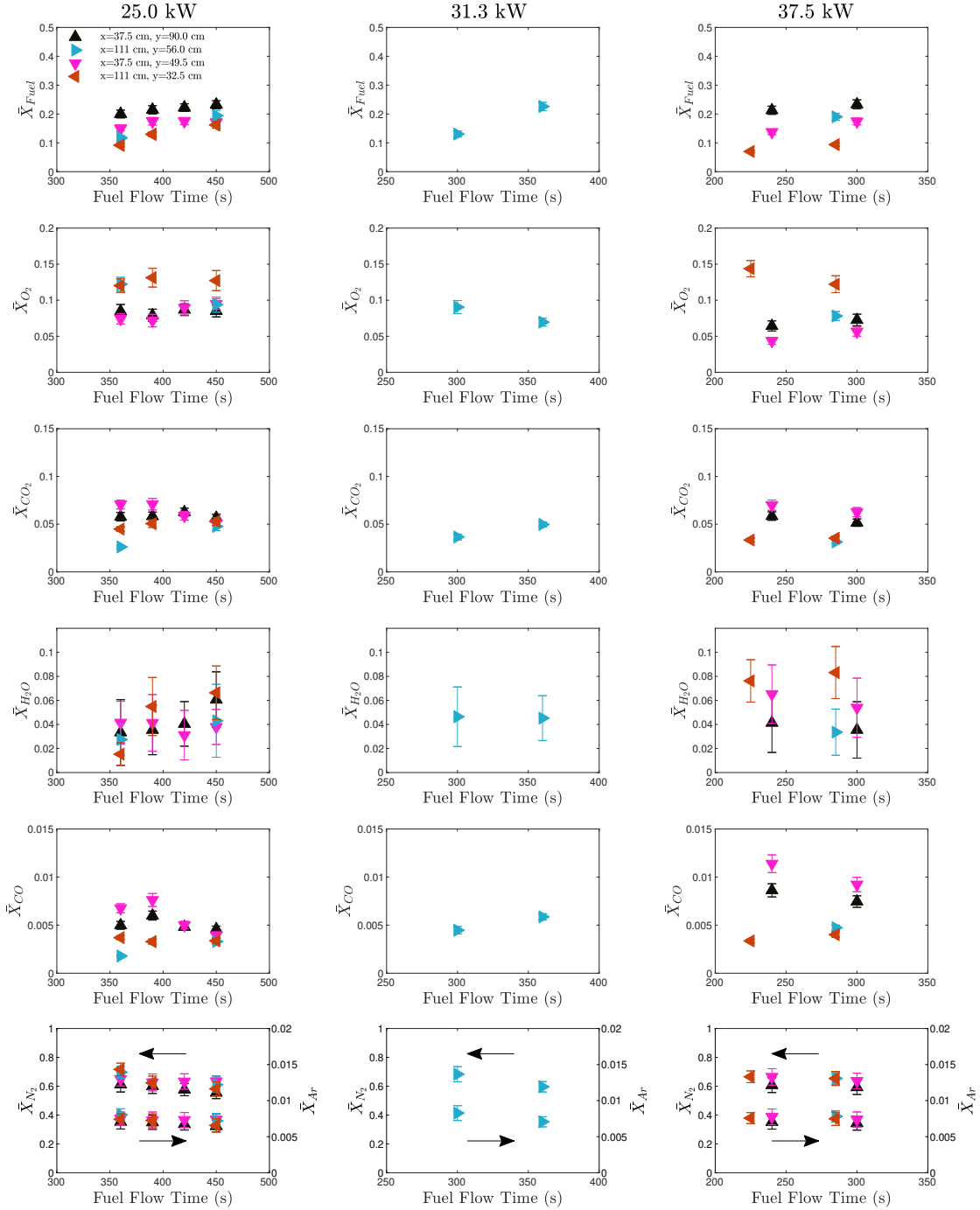


Fig. 15. Time-averaged gas species concentration measurements obtained via GC/MSD of the 25.0 kW, 31.3 kW, and 37.5 kW methane fires with different fuel flow times at different positions within the compartment. The combined uncertainty of the time-averaged gas species concentration measurements is estimated from a combination of the Type A and B evaluations of standard uncertainty. Uncertainty analysis of the time-averaged gas species concentration measurements is provided in Ref [21].

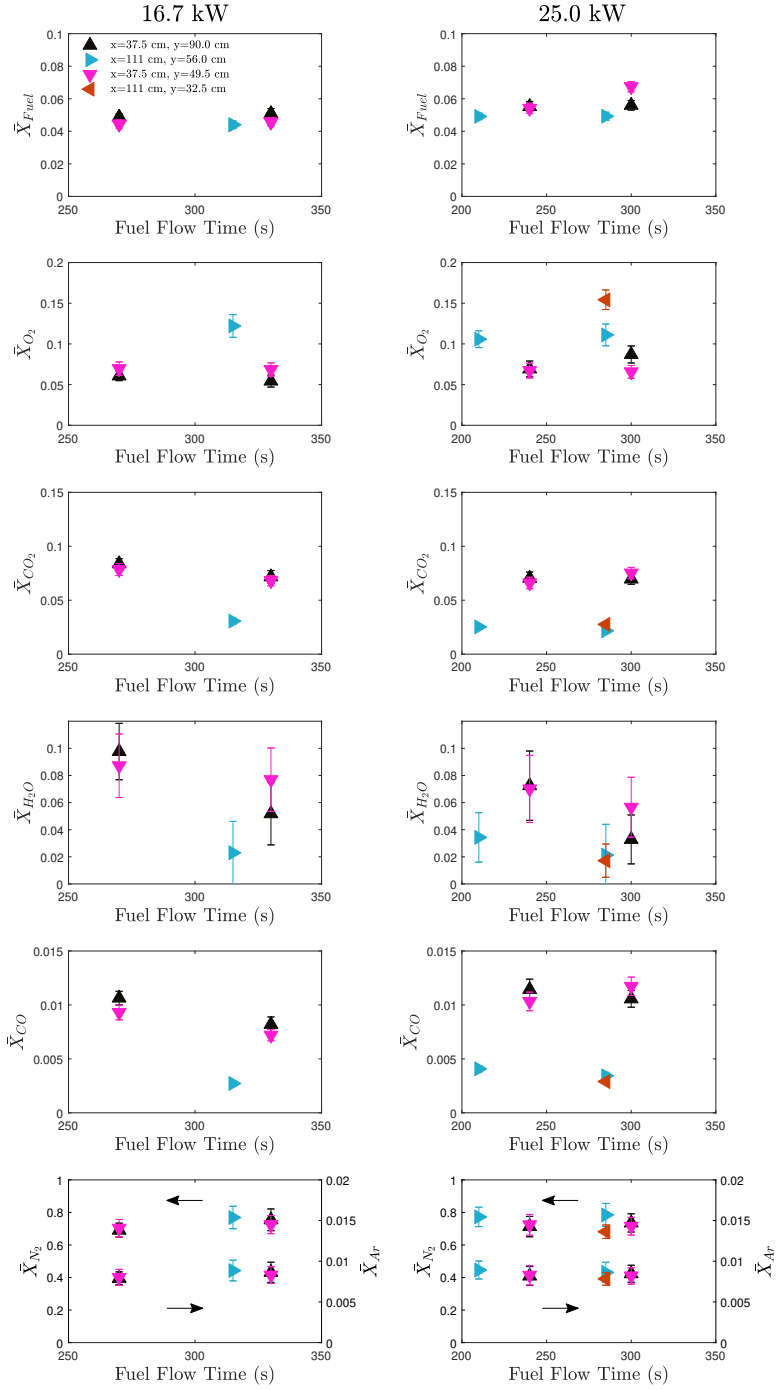


Fig. 16. Time-averaged gas species concentration measurements obtained via GC/MSD of the 16.7 kW, 20.9 kW, and 25.0 kW propane fires with different fuel flow times at different positions within the compartment. The combined uncertainty of the time-averaged gas mixture composition measurements is estimated from a combination of the Type A and B evaluations of standard uncertainty. Uncertainty analysis of the time-averaged gas species concentration measurements is provided in Ref [21].

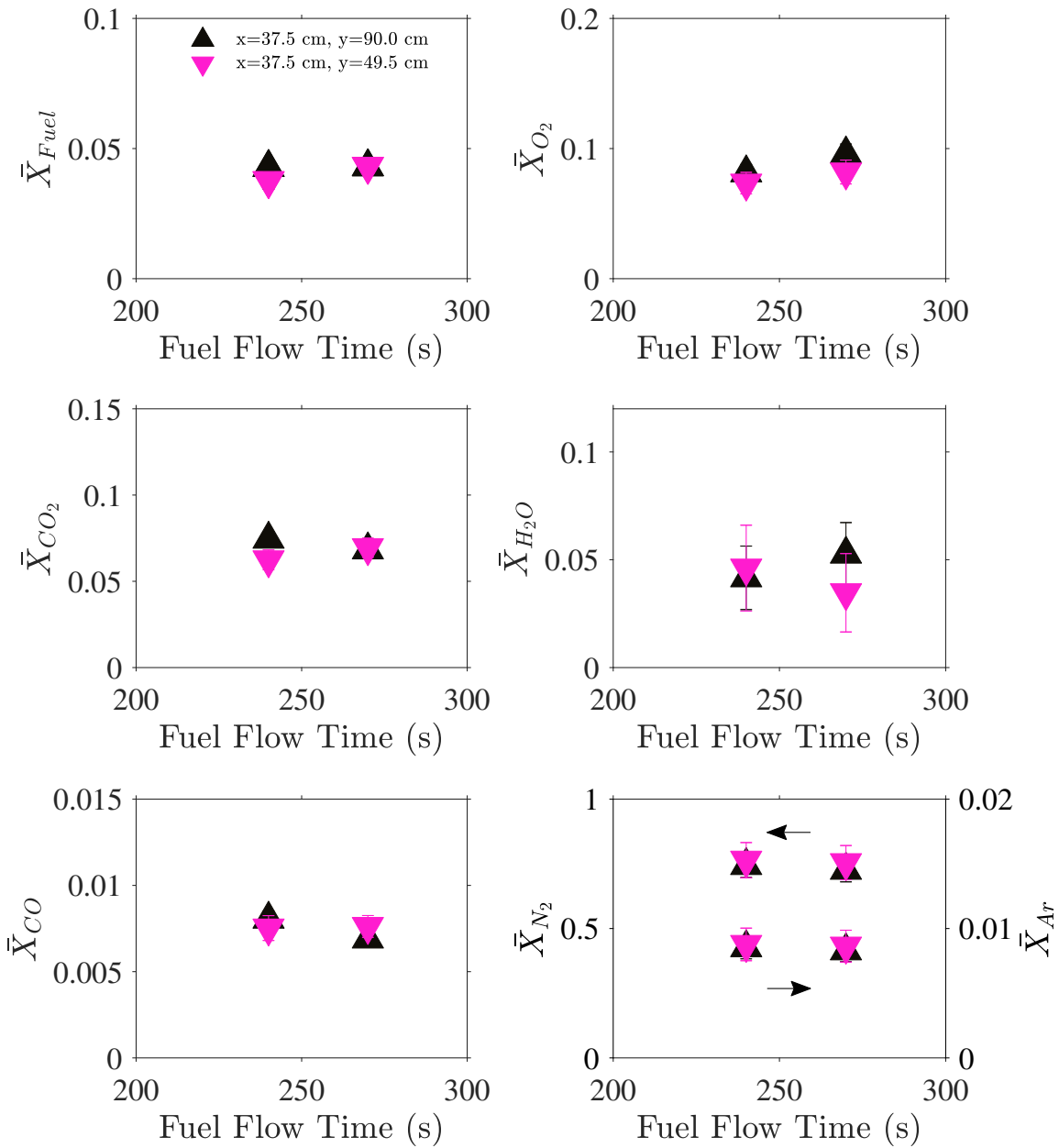


Fig. 17. Time-averaged gas species concentration measurements obtained via GC/MSD of the 25.0 kW propylene fires with different fuel flow times at different positions within the compartment. The combined uncertainty of the time-averaged gas mixture composition measurements is estimated from a combination of the Type A and B evaluations of standard uncertainty. Uncertainty analysis of the time-averaged gas species concentration measurements is provided in Ref [21].

480 4. Verifying Gas Composition Measurements

481 Time-averaged measurements of the global and local equivalence ratios and gas concen-
482 trations of oxygen, carbon dioxide, and carbon monoxide were compared to measurements
483 made via GC/MSD of an extracted gas sample. As discussed in Section 3.2.2, relatively
484 small concentrations of stable hydrocarbons (i.e., ethane, ethylene, acetylene, benzene)
485 were measured for fire configurations and were used to calculate the global and local equiv-
486 alence ratio using Eqs. 3 and 4, respectively. The global equivalence ratio is calculated from
487 GC/MSD measurements via the product of a stoichiometric coefficient and the ratio of the
488 sum of all uncombusted fuels and combustion products to uncombusted oxygen and all
489 combustion products derived from oxygen. The local equivalence ratio is calculated via
490 the ratio between the sum of all unburned fuels and oxygen present in the extracted sample
491 over the stoichiometric ratio of each fuel, assuming one mole of fuel, as shown in Eq. 4.

$$\bar{\phi}_G = \frac{(x + \frac{y}{4} - \frac{z}{2})}{x} \left(\frac{\sum(x + \frac{y}{4} - \frac{z}{2}) \cdot X_{i,C}}{X_{O_2} + X_{CO_2} + 0.5X_{CO} + 0.5X_{H_2O}} \right) \quad (3)$$

$$\bar{\phi}_L = \frac{\sum(x + \frac{y}{4} - \frac{z}{2}) \cdot X_{(C_xH_yO_z)}}{X_{O_2}} \quad (4)$$

492 Here, X_i represents the mole fraction of species i. The mole fraction of fuel is represented
493 by $X_{(C_xH_yO_z)}$ and x, y, and z are the number of carbon, hydrogen, and oxygen atoms in the
494 parent fuel. The concentration of carbon containing species derived from the parent fuel is
495 represented by $X_{i,C}$. Gas concentration measurements obtained using the gas analyzer were
496 compared to GC/MSD concentration measurements recalculated on a dry basis.

497 The comparison between the independent equivalence ratio and gas specie concentration
498 measurements is displayed in Fig. 18 with unity being represented by the dotted line. For
499 most experiments, the time-averaged equivalence ratio estimated from the phi meter and
500 GC/MSD is in fair agreement within experimental uncertainty. The oxygen, carbon diox-
501 ide, and carbon monoxide concentration measurements obtained from the gas analyzer and
502 GC/MSD are also in fair agreement within some experimental uncertainty. The agreement
503 between measurements validates the experimental technique and indicates minimal loss of
504 condensable or semi-volatile species within the heated gas line.

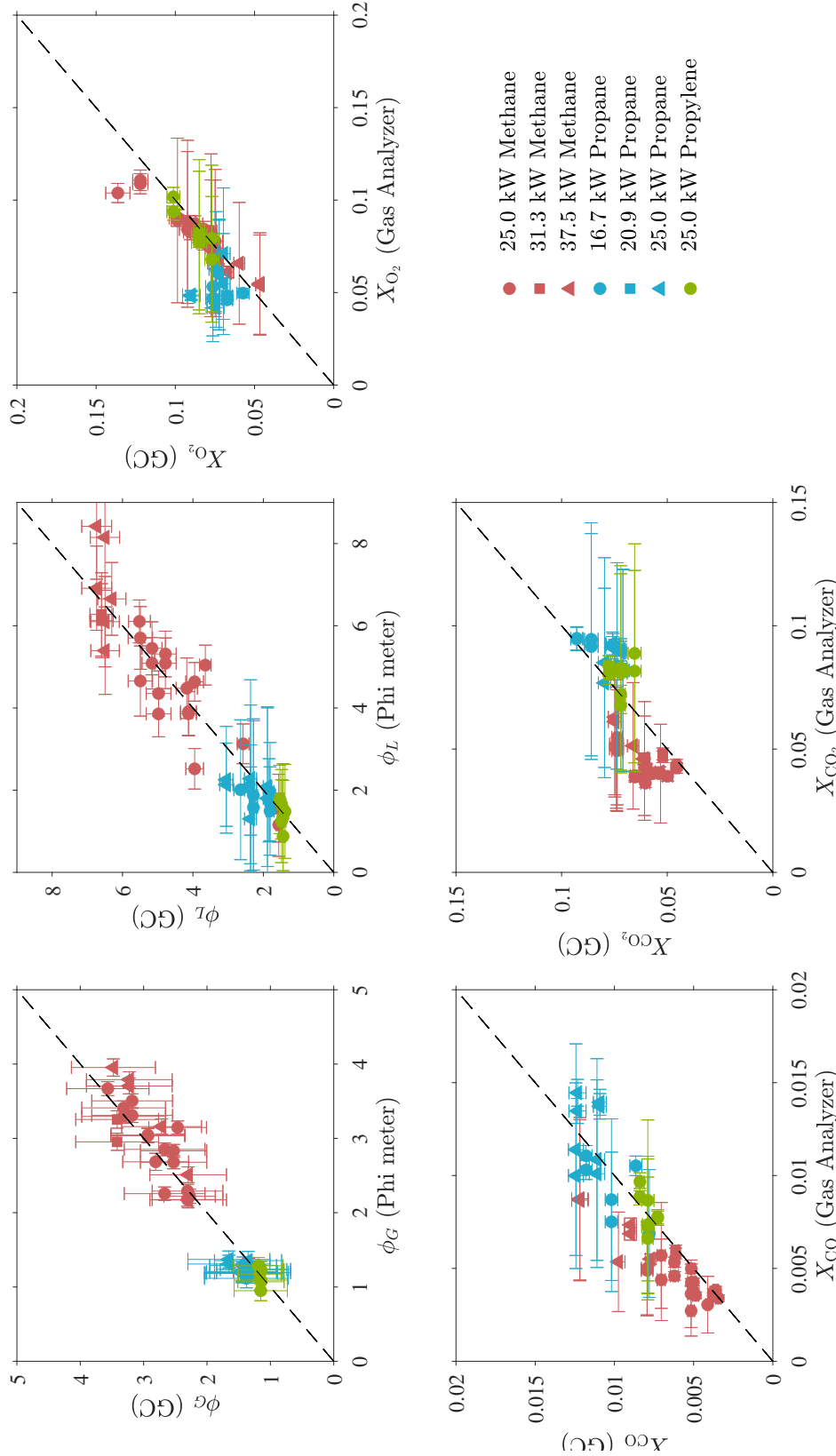


Fig. 18. Time-averaged gas mixture composition measurements were obtained via phi meter and gas analyzer compared to GC/MSD measurements. The provided uncertainties represent a combined Type A and B evaluations of standard uncertainty.

505 **5. Probabilities of Backdraft at varying experimental conditions**

506 The probability of a backdraft under a set compartment configuration (i.e., fuel type, fire
507 size, spark location, doorway opening size) is presented in a series of conditional density
508 plots, Figs. 19-25. Each plot represents the likelihood of backdraft as a function of fuel
509 flow time at a fixed fuel, fire size, "door" or "window" opening configuration, and lower
510 or middle spark location. For all configurations, the probability of backdraft increases
511 with the fuel flow time. Under the same fuel type and fuel flow time, the probability of
512 a backdraft is greater when the spark location is higher in the compartment. Backdraft
513 probabilities are also improved with a "window" opening configuration, 20% smaller than
514 the whole doorway opening. The higher probability of backdraft under the smaller doorway
515 and middle spark location conditions could be attributed to the turbulent mixing of the
516 incoming gravity current, presenting a flammable mixture surrounding the spark igniter.

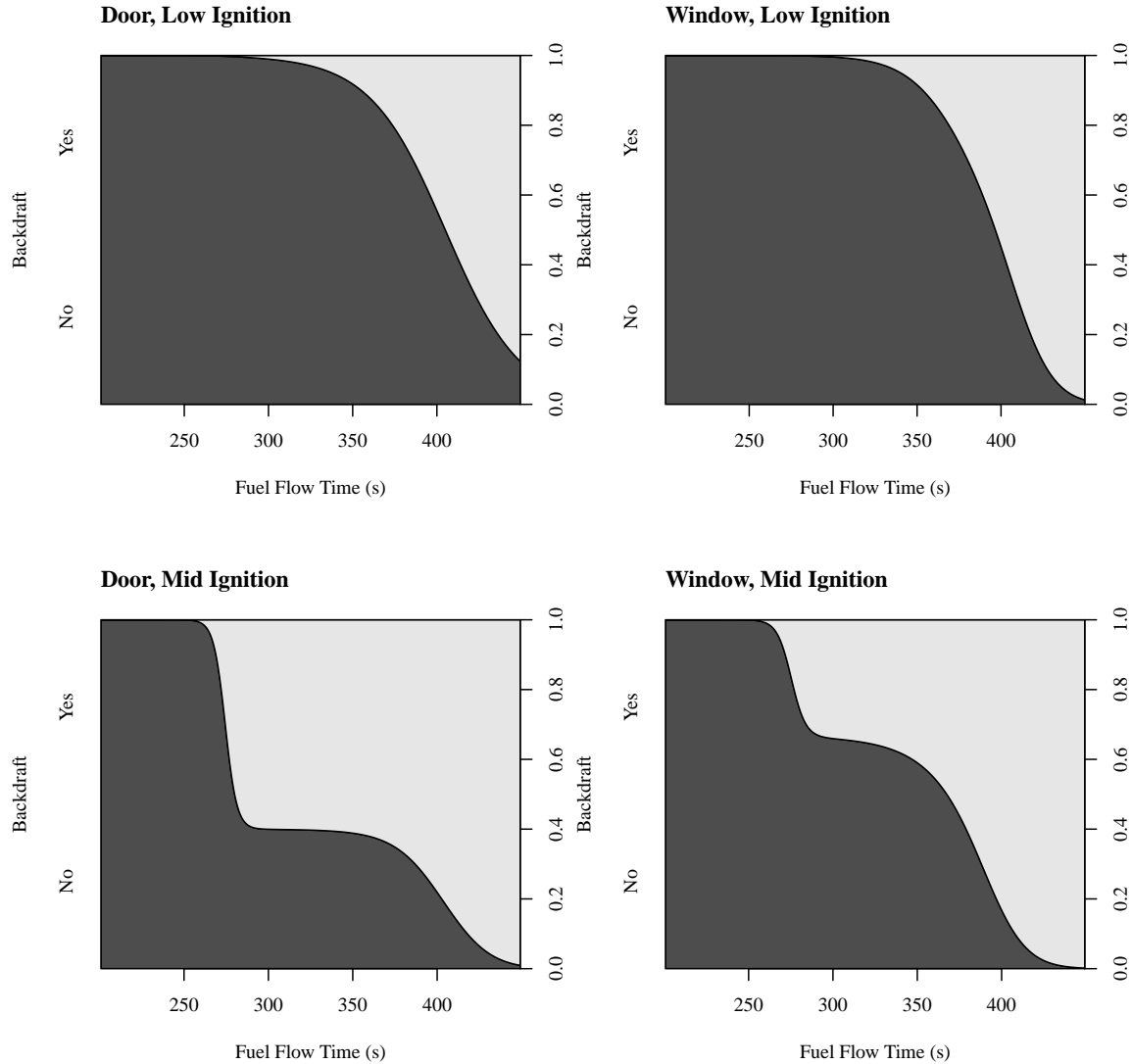


Fig. 19. Conditional density plot of a 25 kW methane fire as a function of fuel flow time at various compartment configurations

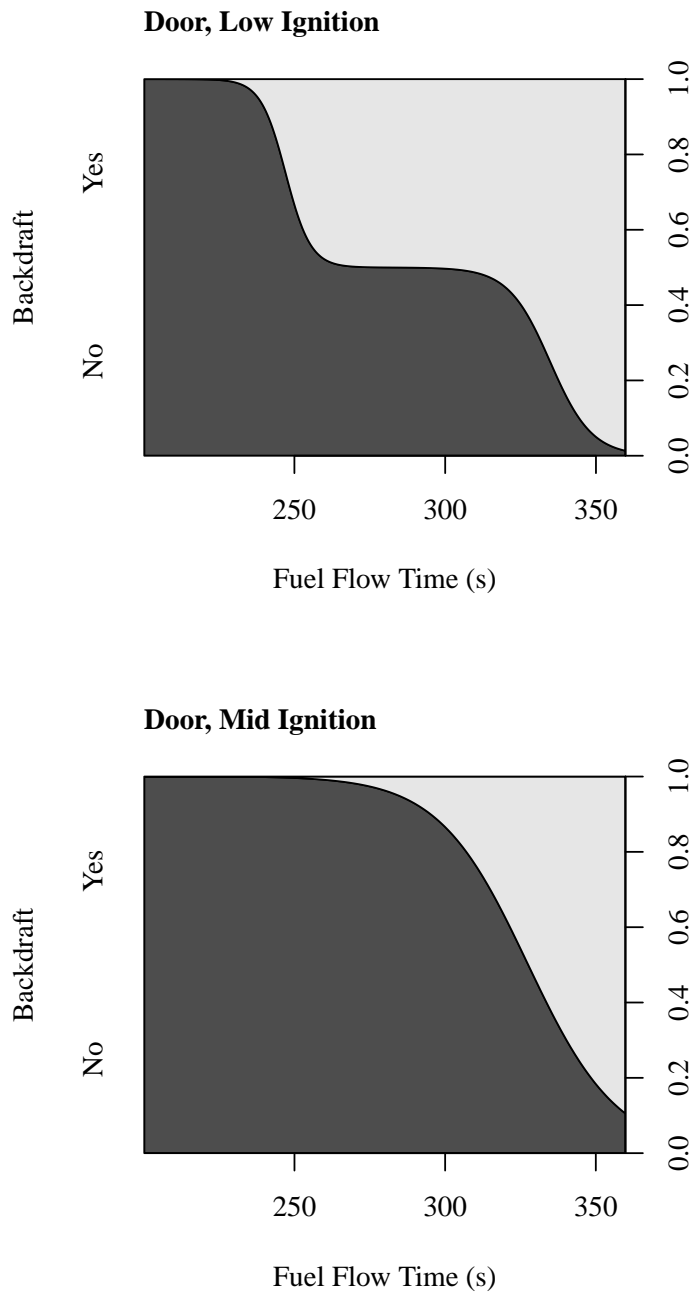


Fig. 20. Conditional density plot of a 31.3 kW methane fire as a function of fuel flow time at various compartment configurations

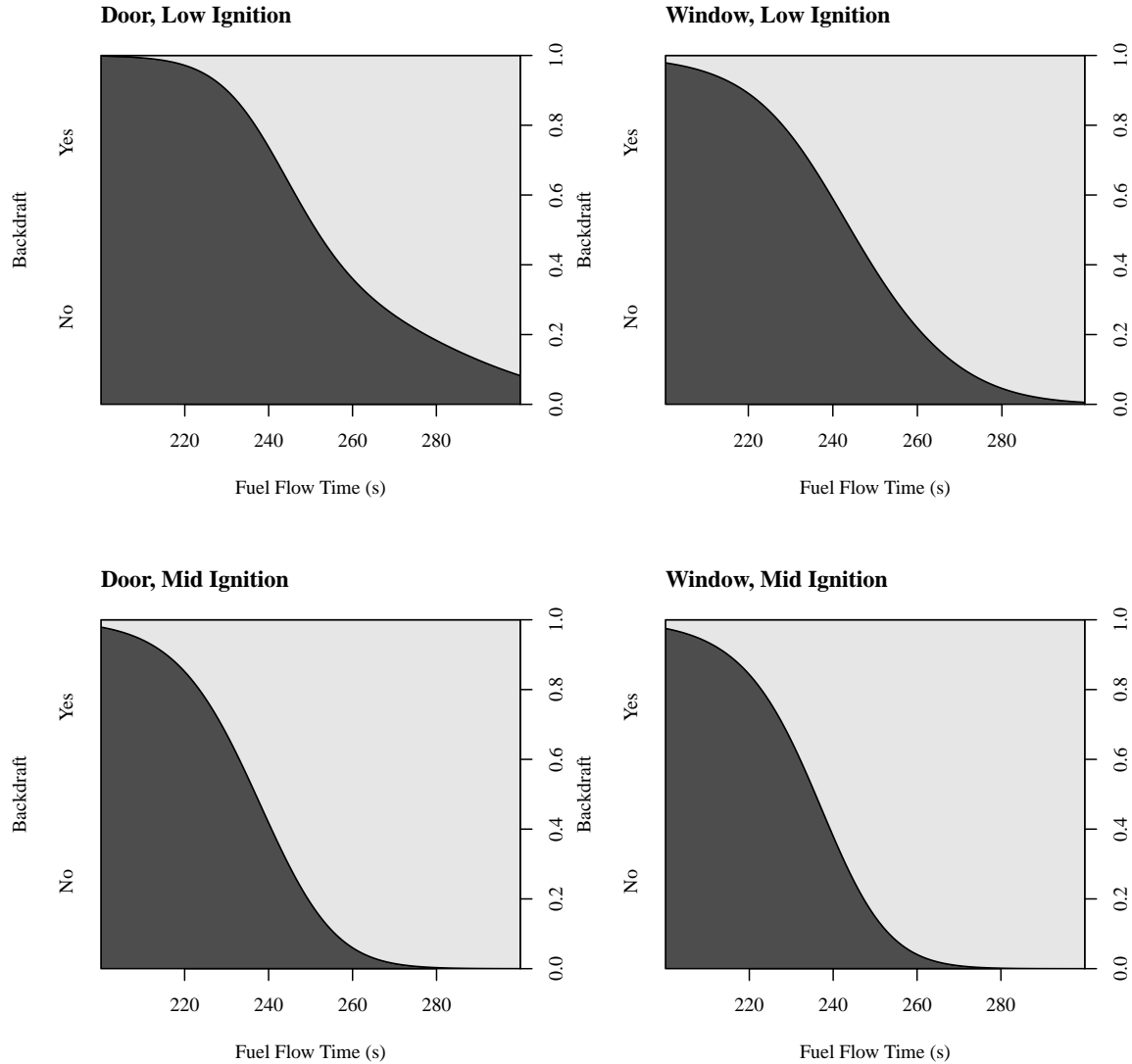


Fig. 21. Conditional density plot of a 37.5 kW methane fire as a function of fuel flow time at various compartment configurations

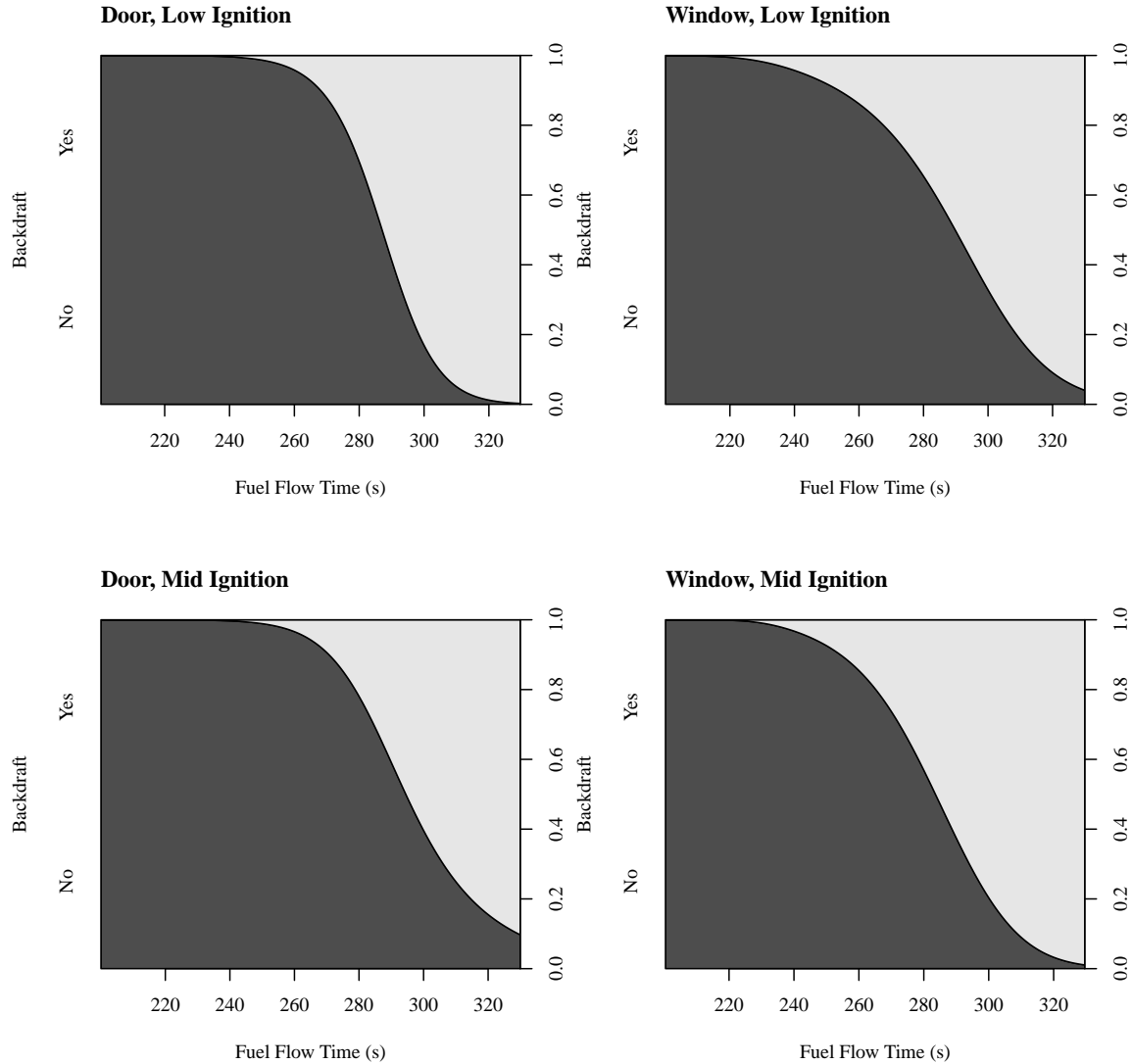


Fig. 22. Conditional density plot of a 16.7 kW propane fire as a function of fuel flow time at various compartment configurations

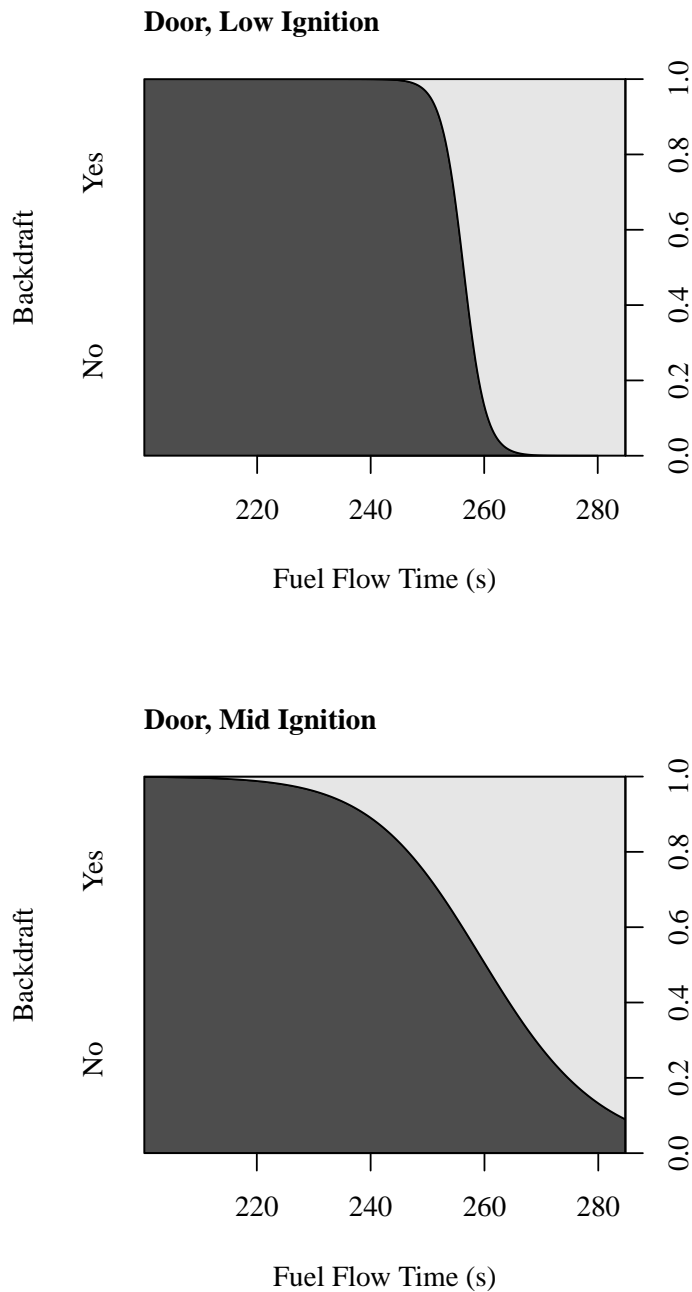


Fig. 23. Conditional density plot of a 20.9 kW propane fire as a function of fuel flow time at various compartment configurations

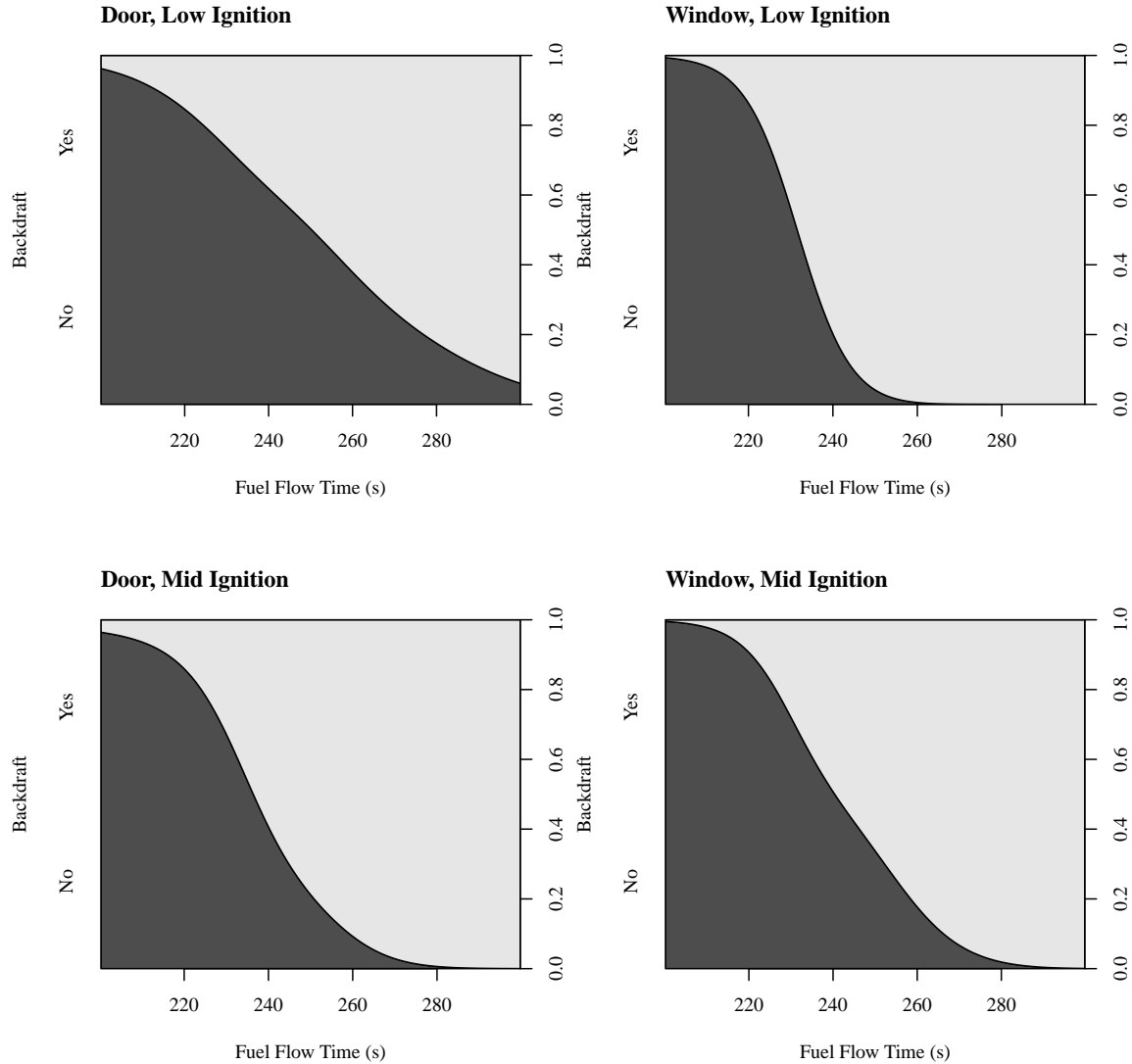


Fig. 24. Conditional density plot of a 25.0 kW propane fire as a function of fuel flow time at various compartment configurations

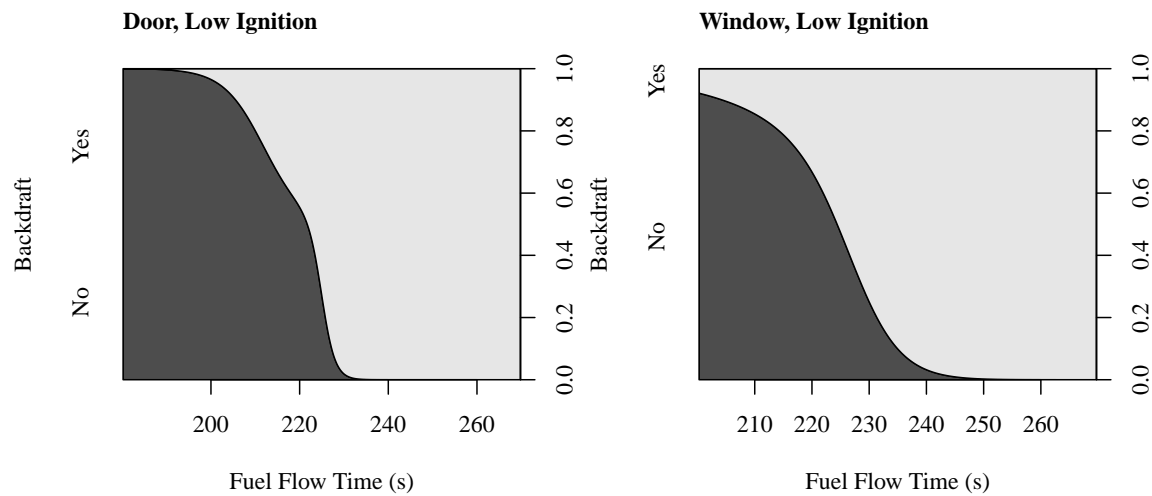


Fig. 25. Conditional density plot of a 25.0 kW propylene fire as a function of fuel flow time at various compartment configurations

517 **6. Conclusion**

518 In summary, real-time and time-averaged measurements of temperature, global and local
519 equivalence ratios, and O₂, CO₂, and CO concentrations on a dry basis are made to charac-
520 terize conditions prior to an anticipated backdraft in an enclosure subjected to various fuel
521 types, fire sizes, and fuel flow times. In instances where methane was utilized, the gas com-
522 position was found to be richer in the upper region of the compartment prior to the doorway
523 opening. For the experiment involving propane and propylene fires, the fuel settled closer
524 to the bottom of the compartment as fuel flow time increased. Gas mixture composition
525 measurements were verified by GC/MSD, which also provided a detailed description of
526 gas species concentration of extracted gas samples from experiments subjected to different
527 conditions. The likelihood of a backdraft was found to increase with fuel flow rate. A
528 smaller opening and higher spark location were also shown to improve the probability of
529 backdraft.

530 **References**

- 531 [1] Fleischmann C (1993) Backdraft phenomena. Ph.D. thesis. University of California,
532 Berkeley, Berkeley, USA, .
- 533 [2] Fleischmann C, Pagni P, Williamson R (1994) Quantitative backdraft experiments.
534 *Fire Safety Science-Proceedings of the Fourth International Symposium*, , pp 337–
535 348.
- 536 [3] Fleischmann C, Pagni P, Williamson R (1993) Exploratory backdraft experiments.
537 *Fire Technology* 29(4):298–316.
- 538 [4] Bollinger I (1995) Full residential-scale backdraft Master's thesis University of Can-
539 terbury, Christchurch, New Zealand.
- 540 [5] Weng W, Fan W (2003) Critical condition of backdraft in compartment fires: a
541 reduced-scale experimental study. *Journal of Loss Prevention in the Process Indus-*
542 *ties* 16(1):19–26.
- 543 [6] Weng W, Fan W (2002) Experimental study on the mitigation of backdraft in com-
544 partment fires with water mist. *Journal of Fire Sciences* 20(4):259–278.
- 545 [7] Gottuk D, Peatross M, Farley J, Williams F (1999) The development and mitigation
546 of backdraft: a real-scale shipboard study. *Fire Safety Journal* 33(4):261–282.
- 547 [8] Gottuk D, Williams F, Farley J (1997) The development and mitigation of backdrafts:
548 a full-scale experimental study. *Fire Safety Science* 5:935–946.
- 549 [9] Gojkovic D (2000) Initial backdraft experiments (Lund University), 3121.
- 550 [10] Tsai L, Chiu C (2013) Full-scale experimental studies for backdraft using solid mate-
551 rials. *Process Safety and Environmental Protection* 91(3):202–212.
- 552 [11] Chen N (2012) Smoke Explosion in Severally Ventilation Limited Compartment Fires
553 Master's thesis University of Canterbury, Christchurch, New Zealand.
- 554 [12] Parkes A (2009) The Impact of Size and Location of Pool Fires on Compartment Fire
555 Behaviour. Ph.D. thesis. University of Canterbury, Christchurch, New Zealand, .
- 556 [13] Park J, Oh C, Choi B, Han Y (2015) Computational visualization of the backdraft
557 development process in a compartment. *Journal of Visualization* 18(1):25–29.
- 558 [14] Ferraris S, Wen J, Dembele S (2008) Large eddy simulation of the backdraft phe-
559 nomenon. *Fire Safety Journal* 43(3):205–225.
- 560 [15] Weng W, Fan W, Hasemi Y (2005) Prediction of the formation of backdraft in a
561 compartment based on large eddy simulation. *Engineering Computations* 22(4):376–
562 392.
- 563 [16] Park J, Oh C, Han Y, Do K (2017) Computational study of backdraft dynamics and
564 the effects of initial conditions in a compartment. *Journal of Mechanical Science and*
565 *Technology* 31(2):985–993.
- 566 [17] Horvat A, Sinai Y (2007) Numerical simulation of backdraft phenomena. *Fire Safety*
567 *Journal* 42(3):200–209.
- 568 [18] Bryant R, Ohlemiller T, Johnsson E, Hamins A, Grove B, Guthrie W, Maranghides
569 A, Mulholland G (2003) The NIST 3 megawatt quantitative heat release rate facility
570 (National Institute of Standards and Technology), NIST Special Publication 1001.

- 571 [19] Cleary T, Falkenstein-Smith R, Brown C (2021) Evolution and characterization of
572 backdraft hazard in a 2/5th scale compartment. *Proc. of the 12th Asia-Oceania Sym-*
573 *posium on Fire Science and Technology*, . .
- 574 [20] Brown C, Falkenstein-Smith R, Cleary T (2021) Reduced-Scale Compartment
575 Gaseous Fuels Backdraft Experiments (National Institute of Standards and Technol-
576 ogy), NIST Technical Note 2183.
- 577 [21] Falkenstein-Smith R, Sung K, Chen J, Harris K, Hamins A (2021) The Structure
578 of Medium-Scale Pool Fires, Second Edition (National Institute of Standards and
579 Technology), NIST Technical Note 2082,e2.
- 580 [22] Falkenstein-Smith R, Harris K, Sung K, Liang T, Hamins A (2021) A calibration
581 and sampling technique for quantifying the chemical structure in fires using gc/msd
582 analysis. *Fire and Materials* .
- 583 [23] Babrauskas V, Parker W, Mulholland G, Twilley W (1994) The phi meter: A simple,
584 fuel-independent instrument for monitoring combustion equivalence ratio. *Review of*
585 *Scientific Instruments* 65(7):2367–2375.
- 586 [24] Falkenstein-Smith R, Cleary T (2021) The Design and Performance of a Second-
587 Generation Phi Meter (National Institute of Standards and Technology), NIST Tech-
588 nical Note 2184.
- 589 [25] Stavropoulos P, Michalakou A, Skevis G, Couris S (2005) Quantitative local equiv-
590 alence ratio determination in laminar premixed methane-air flames by laser induced
591 breakdown spectroscopy (LIBS). *Chemical Physics Letters* 404(4-6):309–314.
- 592 [26] Han D, Steeper R (2002) An LIF equivalence ratio imaging technique for multicom-
593 ponent fuels in an ic engine. *Proceedings of the Combustion Institute* 29(1):727–734.
- 594 [27] Hurley M (ed) (2016) *SFPE Handbook of Fire Protection Engineering* (Springer, New
595 York), 5th Ed.

596 Appendix A. Uncertainty Analysis of Real-time Measurements

597 Appendix A.1. Temperature

598 The uncertainty of thermocouple measurements is estimated from the Type B evaluation
599 of standard uncertainty determined from the thermocouple error, which is approximately
600 2.20 °C or 0.75% of the reading, whichever is greater. A coverage factor of 2 is applied to
601 the combined uncertainty to produce a 95 % confidence interval.

**602 Appendix A.2. Gas Species Concentration Measurements obtained via Gas
603 Analyzer**

604 The uncertainty of individual gas species concentration measurements is estimated from the
605 Type B evaluation of standard uncertainty defined by the bias in the instrumentation. For
606 direct gas analyzer measurements, the uncertainty attributed to the instrument is provided
607 in Table 2. A coverage factor of 2 is applied to the combined uncertainty to produce a 95 %
608 confidence interval.

Table 2. List of uncertainties for gas analyzer components.

Components	Manufacturer	Rel. Uncertainty (%)
Paramagnetic O ₂ Sensor	California Analytical Instruments, Inc.	2.0
NDIR CO ₂ Sensor	California Analytical Instruments, Inc.	4.0
NDIR CO Sensor	California Analytical Instruments, Inc.	4.0

609 Appendix A.3. Global Equivalence Ratio

610 As shown in Eq. 1, real-time measurements of the global equivalence ratio, ϕ_G , is de-
611 termined from a combination of the volumetric flow reading of the dried exhaust stream,
612 \dot{V}_{MFC} , the O₂ and CO₂ concentrations within the dried exhaust stream, X_{O_2} and X_{CO_2} , and
613 the volumetric flow of excess oxygen introduced in the phi meter's reactor, $\dot{V}_{O_2,Ex}$. The
614 uncertainty of the global equivalence ratio is estimated using the law of propagation of
615 uncertainty:

$$u_{\phi_G} = \sqrt{\left(\frac{\partial \phi_G}{\partial \dot{V}_{MFC}} u_{\dot{V}_{MFC}} \right)^2 + \left(\frac{\partial \phi_G}{\partial X_{O_2}} u_{X_{O_2}} \right)^2 + \left(\frac{\partial \phi_G}{\partial X_{CO_2}} u_{X_{CO_2}} \right)^2 + \left(\frac{\partial \phi_G}{\partial \dot{V}_{O_2,Ex}} u_{\dot{V}_{O_2,Ex}} \right)^2} \quad (5)$$

616 The volume fraction of oxygen in the air, $X_{O_2,Ent}$, is included in Eq. 1 and is assumed to be
617 constant and therefore does not affect the global equivalence ratio uncertainty. A coverage
618 factor of 2 is applied to the combined uncertainty to produce a 95 % confidence interval.

619 The uncertainty of the concentration and flow measurements in Eq. 5 are defined as the
 620 Type B evaluation of standard uncertainty, determined from the instrument error provided
 621 by the manufacturer. Table 3 provides a summary of instruments incorporated into the phi
 622 meter that are used to determine ϕ_G .

Table 3. List of uncertainties for selected phi meter components.

Components	Manufacturer	Rel. Uncertainty (%)
High-Temperature Mass Flow Controller	Alicat Scientific, Inc.	0.2
Oxygen Mass Flow Controller	Brooks Instrument	2.0
Mass Flow Meter	Alicat Scientific, Inc.	0.2
Paramagnetic O ₂ Sensor	Servomex Group Ltd.	0.5
NDIR CO ₂ Sensor	Servomex Group Ltd.	4.0

623 **Appendix A.4. Local Equivalence Ratio**

624 Real-time measurements of the local equivalence ratio are calculated via Eq. 2, which in-
 625 corporates the mass flows of O₂ in the excess oxygen line, $\dot{m}_{O_2,Ex.}$, the inlet of the phi
 626 meter, $\dot{m}_{O_2,Samp.}$, and the outlet of the phi meter's reactor, $\dot{m}_{O_2,O}$. The uncertainty of the
 627 local equivalence ratio is estimated from the law of propagation of uncertainty:

$$u_{\phi_L} = \sqrt{\left(\frac{\partial \phi_L}{\partial \dot{m}_{O_2,Ex.}} u_{\dot{m}_{O_2,Ex.}} \right)^2 + \left(\frac{\partial \phi_L}{\partial \dot{m}_{O_2,Samp.}} u_{\dot{m}_{O_2,Samp.}} \right)^2 + \left(\frac{\partial \phi_L}{\partial \dot{m}_{O_2,O}} u_{\dot{m}_{O_2,O}} \right)^2} \quad (6)$$

628 The uncertainty of the oxygen mass flow rates are estimated from the Type B evaluation of
 629 standard uncertainty, reported in Ref. [24].

630 **Appendix B. Uncertainty Analysis of Time-Averaged Measurements**

631 The uncertainty of time-averaged measurements, $u_{\bar{i}}$ is determined from a combined Type A
632 and B evaluations of standard uncertainty. The Type A evaluation of standard uncertainty of
633 measurements is calculated from the standard error of the averaged readings, s_i . The Type
634 B evaluation of standard uncertainty of measurements is defined from the bias error sources
635 in the instrumentation, u_{inst} . The combined uncertainty of the time-averaged measurements
636 if found via quadrature:

$$u_{\bar{i}} = \sqrt{s_i^2 + u_{\text{inst}}^2} \quad (7)$$

637